MICHIGAN ENGINEERING
UNIVERSITY OF MICHIGAN

Louise Willingale
The CERN Accelerator School, High Gradient Wakefield Accelerators
Sesimbra, Portugal, 18th February 2019

Laser driven acceleration of protons and ions

(disclaimer: a snapshot from my perspective!)

Why study high intensity laser-plasma interactions?

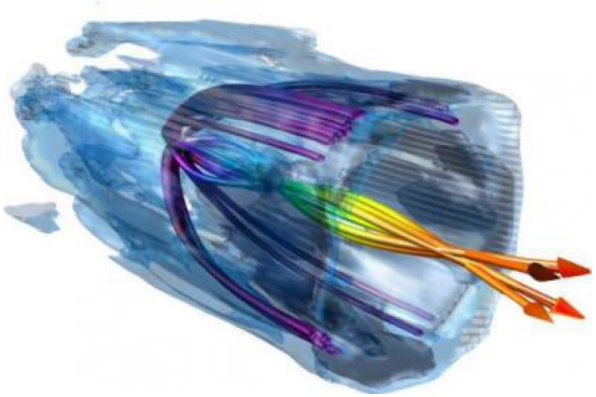

Electron beam generation

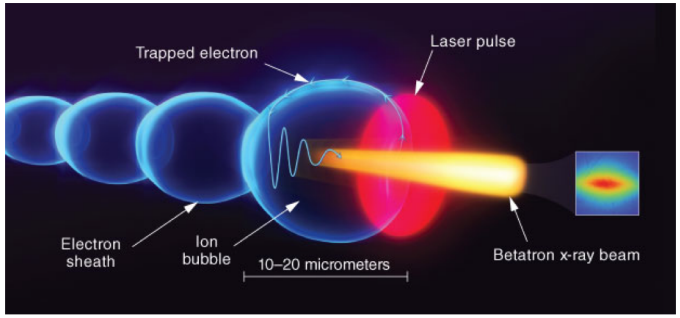

Bright high-energy photon sources

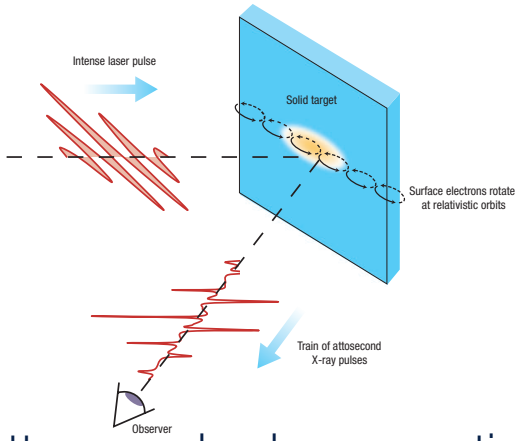

Attosecond pulse generation

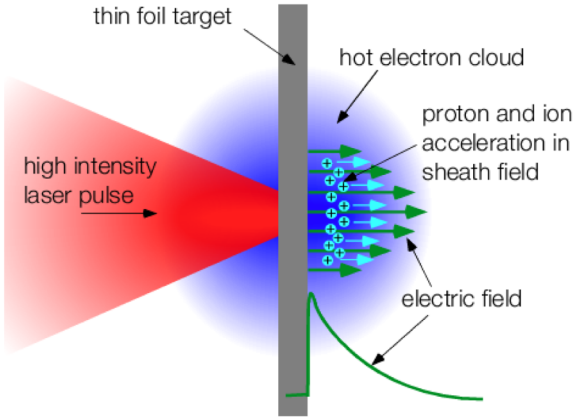

Ion beam generation

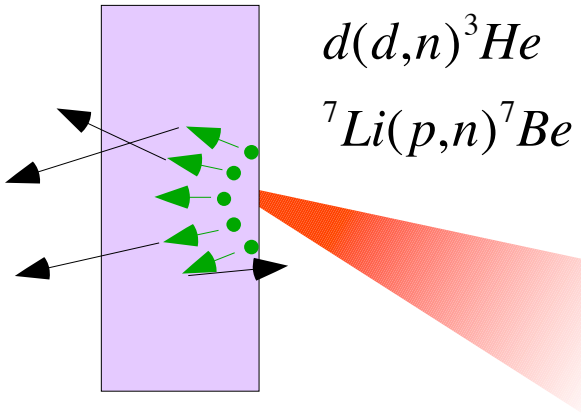

Neutron beam generation

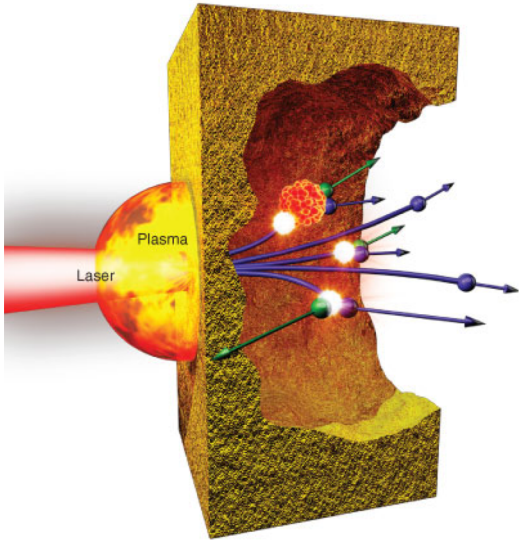

Positron production

Laser-driven ion acceleration

- Motivation / potential applications
- Acceleration mechanism summary
  - Target Normal Sheath Acceleration (TNSA)
  - Advanced mechanisms: RPA, BOA, Magnetic vortex, Shock
- Common physics themes
- Theoretical models to describe TNSA
- Electron heating and fast electron transport
- Proton and ion diagnostics
- TNSA proton beam properties, scaling and other effects
- Laser-driven proton beam application examples

Potential applications of laser driven ion acceleration

Medical applications:
Hadron therapy
PET isotope production

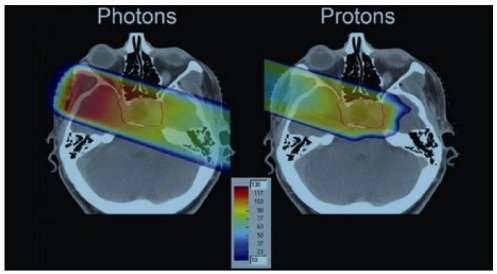

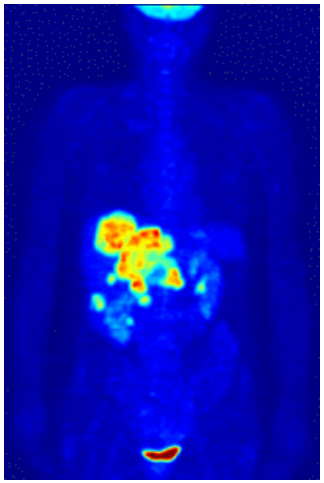

Radiography of High-Energy-Density experiments

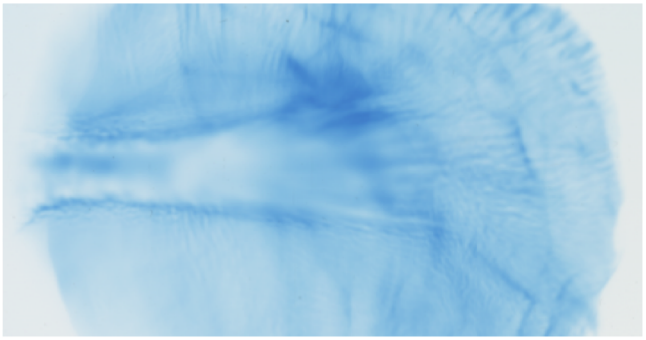

Neutron Spallation source

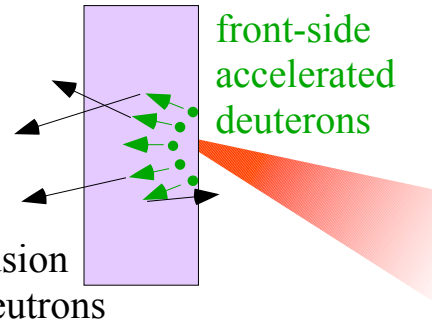

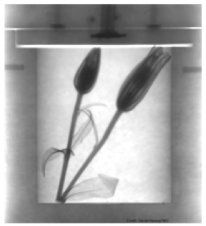

Isochoric heating of material, or energy source for fast ignition inertial confinement fusion

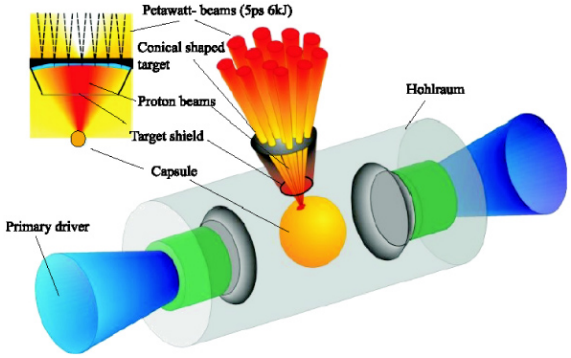

Ion acceleration mechanism: Target Normal Sheath Acceleration (TNSA)

S Hatchett, et al, PoP, 7, 2076 (2000)

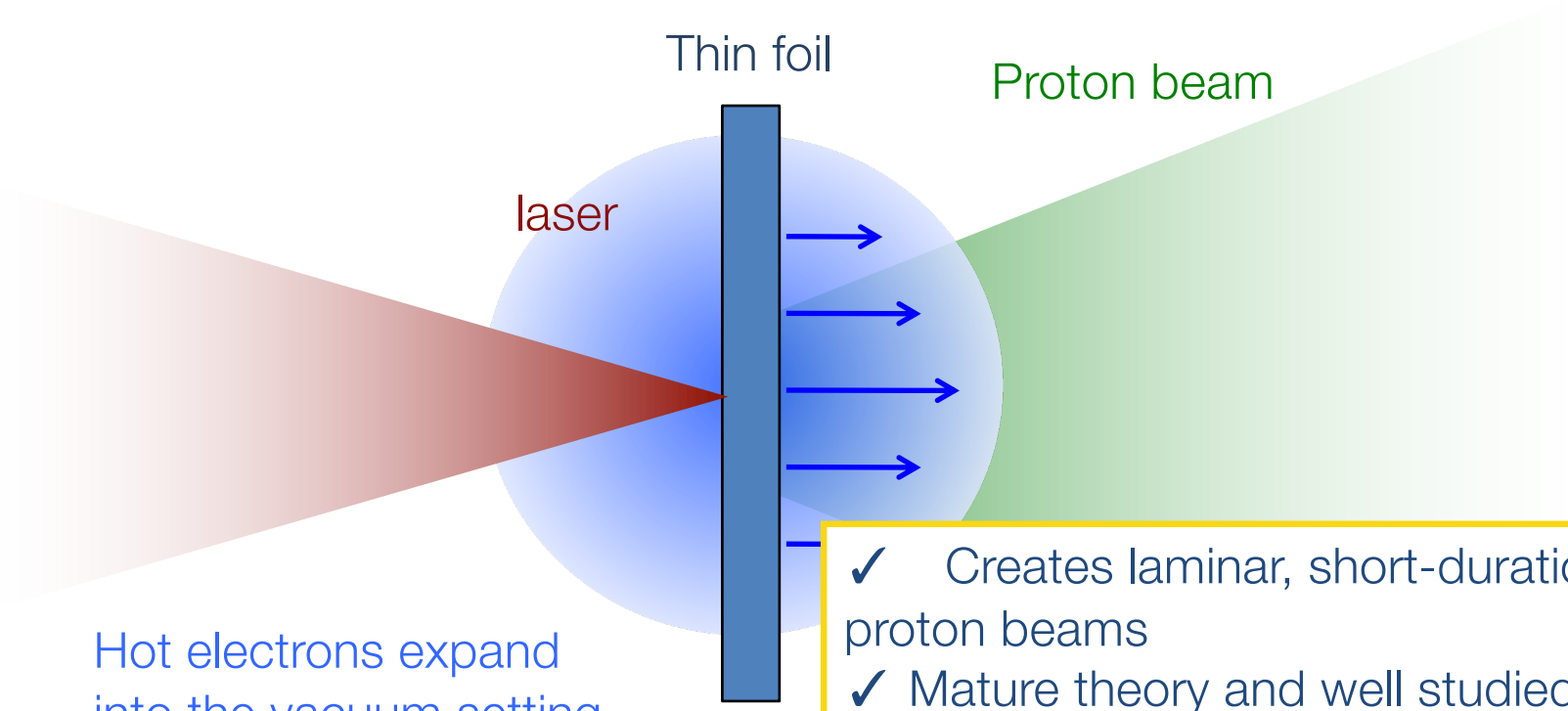

✓ Creates laminar, short-duration, high-flux proton beams
✓ Mature theory and well studied mechanism
✓ Robust enough to explore applications

Energy conversion efficiency ~ few %

✗ Broad, Maxwellian-like energy spread
✗ Maximum ion energy scale with laser energy

Ion acceleration mechanisms: Small energy spread using TNSA?

Structured targets

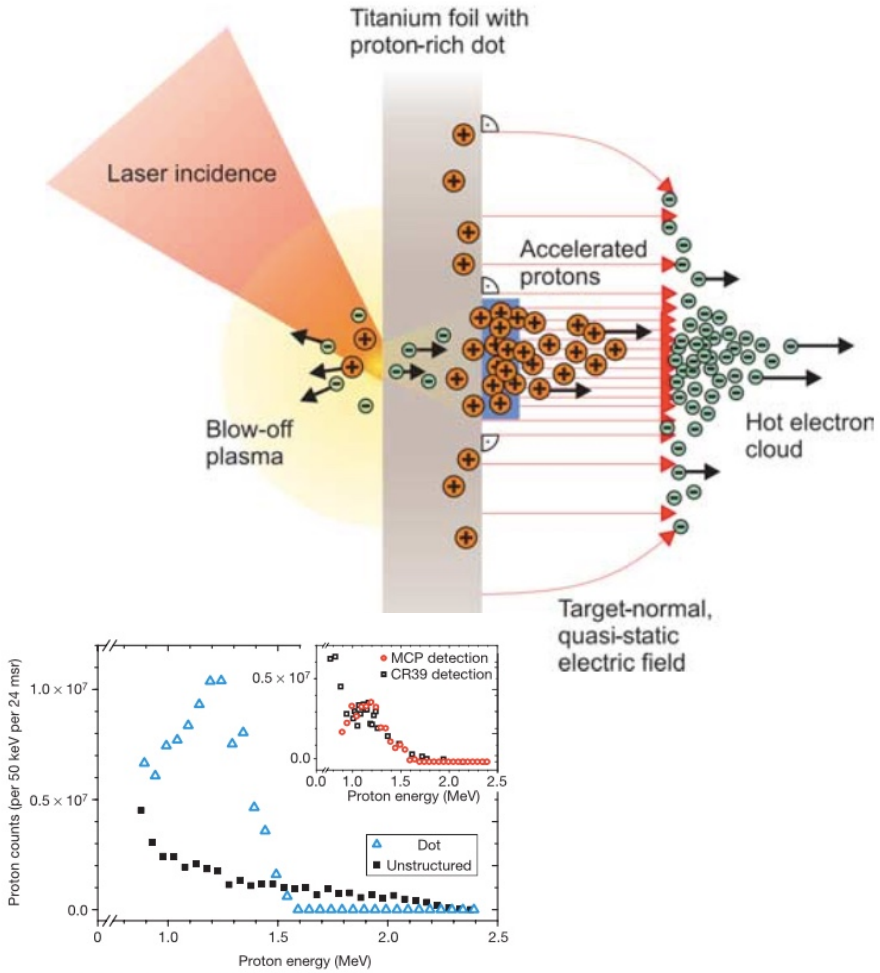

H Schwoerer, et al, Nature, 439, 445 (2006); APL Robinson and P Gibbon, PRE, 75, 015401 (2007)

Complex target preparation:

"an ultrathin layer of graphitic carbon, formed from catalytic decomposition of adsorbed hydrocarbon impurities on a 20 mm palladium foil."

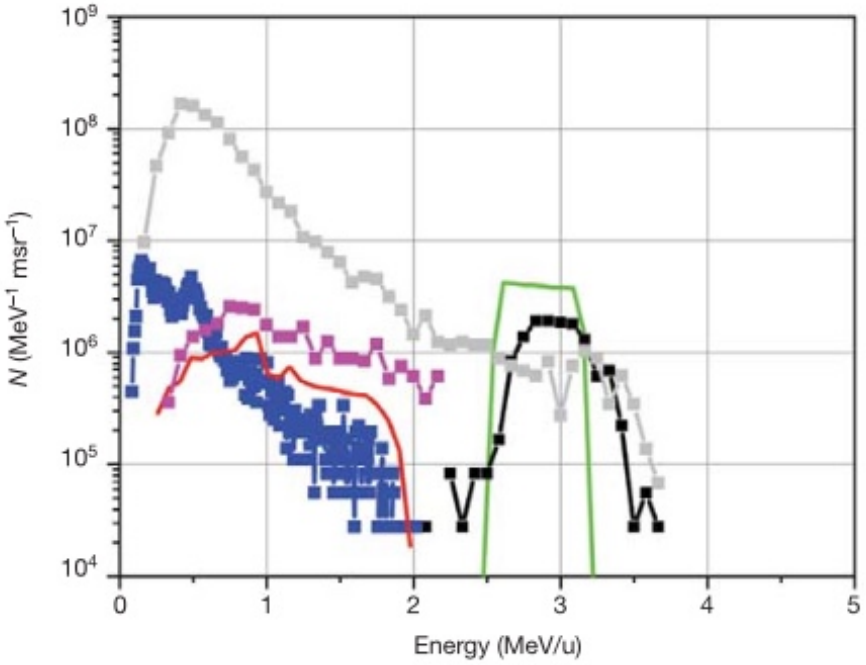

BM Hegelich, et al, Nature, 439, 441 (2006)

Ion acceleration mechanisms: Small energy spread using TNSA?

Use energy selection to achieve quasi-monoenergetic proton spectra

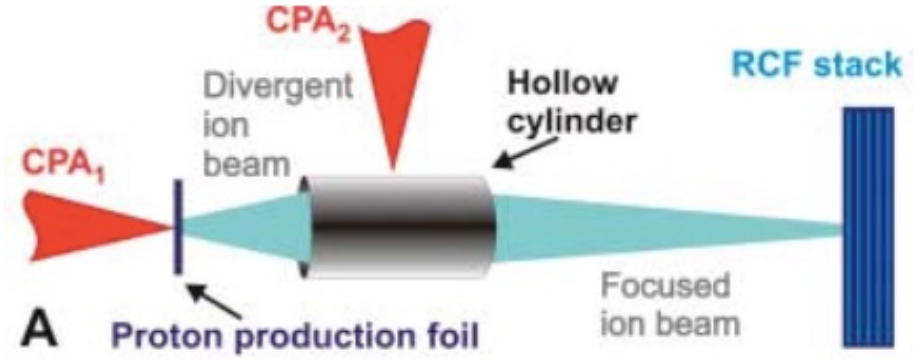

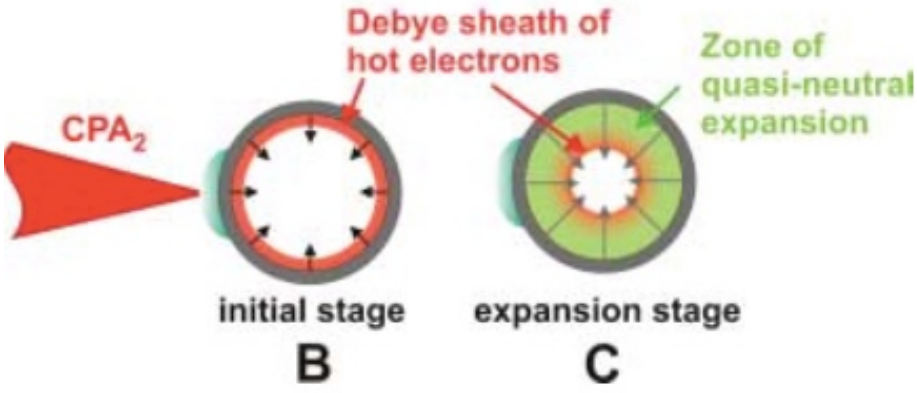

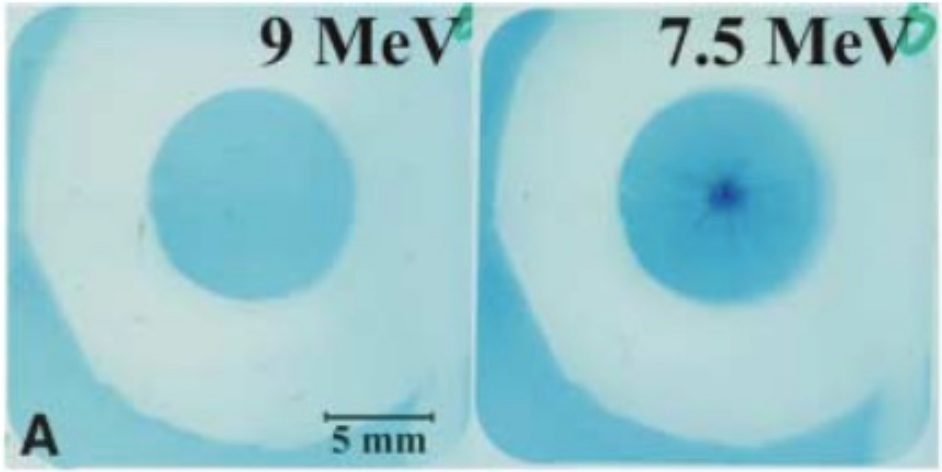

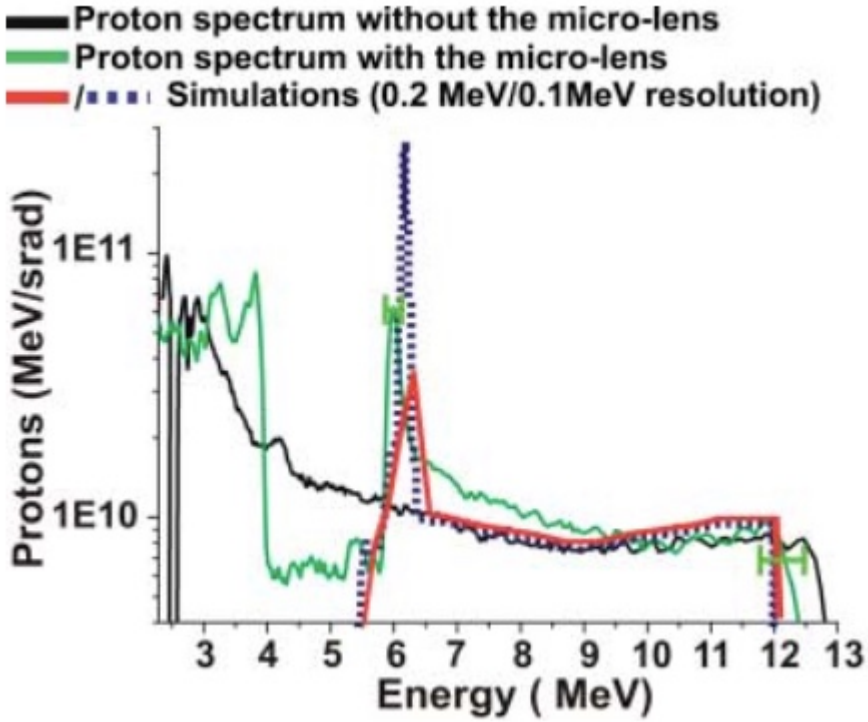

T Toncian, et al, Science, 312, 410 (2006)

Advanced ion acceleration mechanisms: Radiation Pressure Acceleration (RPA)

A Henig, et al, PRL, 103, 245003 (2009)

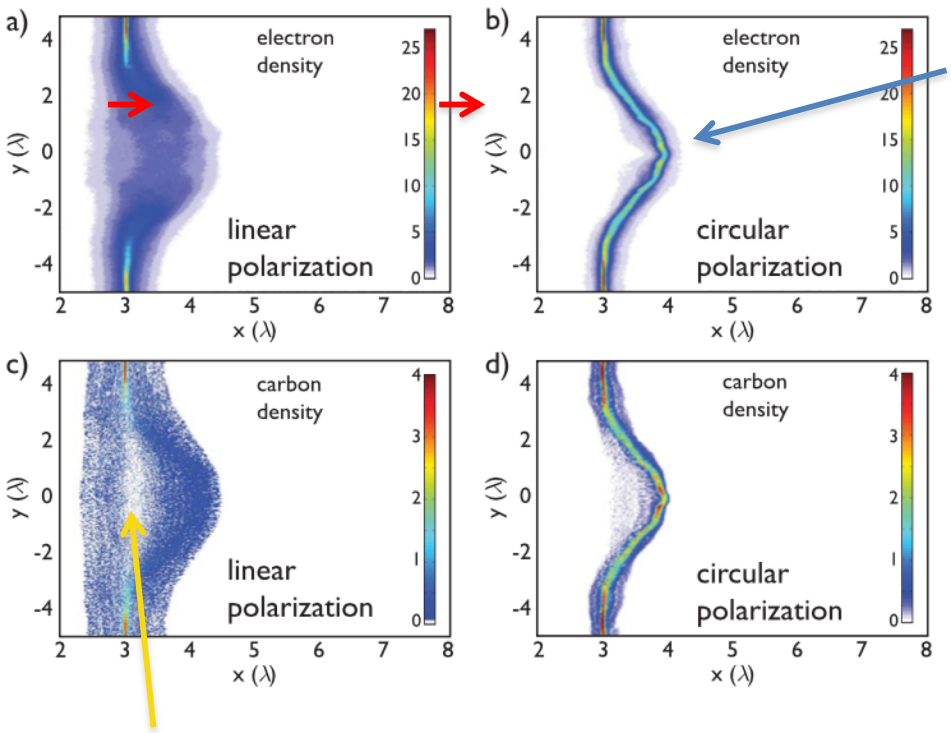

Linear polarization heats electrons strongly and explodes foil, preventing the "light-sail" from forming – TNSA instead.

Laser light pressure pushes entire electron volume of a very thin foil forward forming the acceleration field:

"Light Sail" regime

The ions follow the electrons – all experience same field → same final energy.

✓ Excellent ion energy scaling with laser intensity

✓ Excellent energy conversion efficiency

✓ Quasi-monoenergetic acceleration

✗ Very thin targets difficult to handle

✗ Requires challenging laser parameters:

- Very small laser pre-pulse
- Circular polarization
- Large focal spot, increases the laser energy required

✗ Experimental demonstrations have been so far disappointing

Esirkepov, et al, PRL, 92, 175003 (2004)

Relativistically Induced Transparency

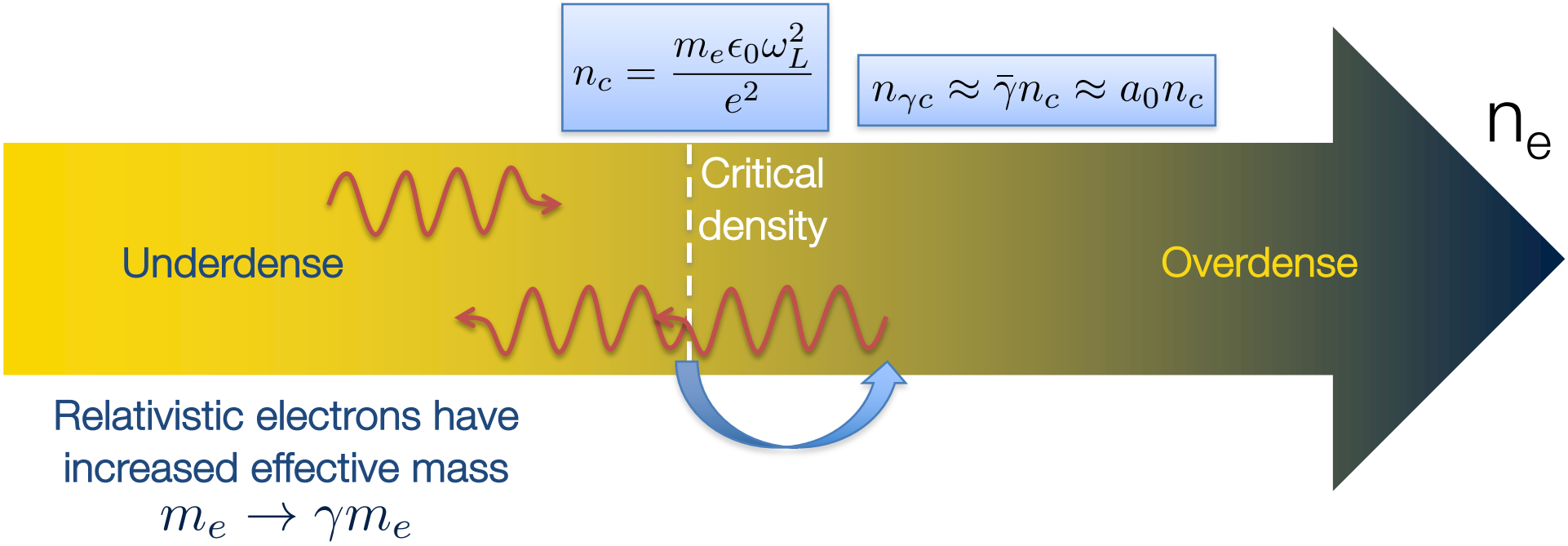

$\bar{\gamma}$ scales as $\approx \gamma_x \approx a_0$

Current state-of-the-art: $a_0 < 50$

Next generation: $a_0 < 300$

Advanced ion acceleration mechanisms: Break-Out Afterburner (BOA)

An initially solid-density target undergoes relativistically induced transparency, initialing a period of enhanced ion acceleration

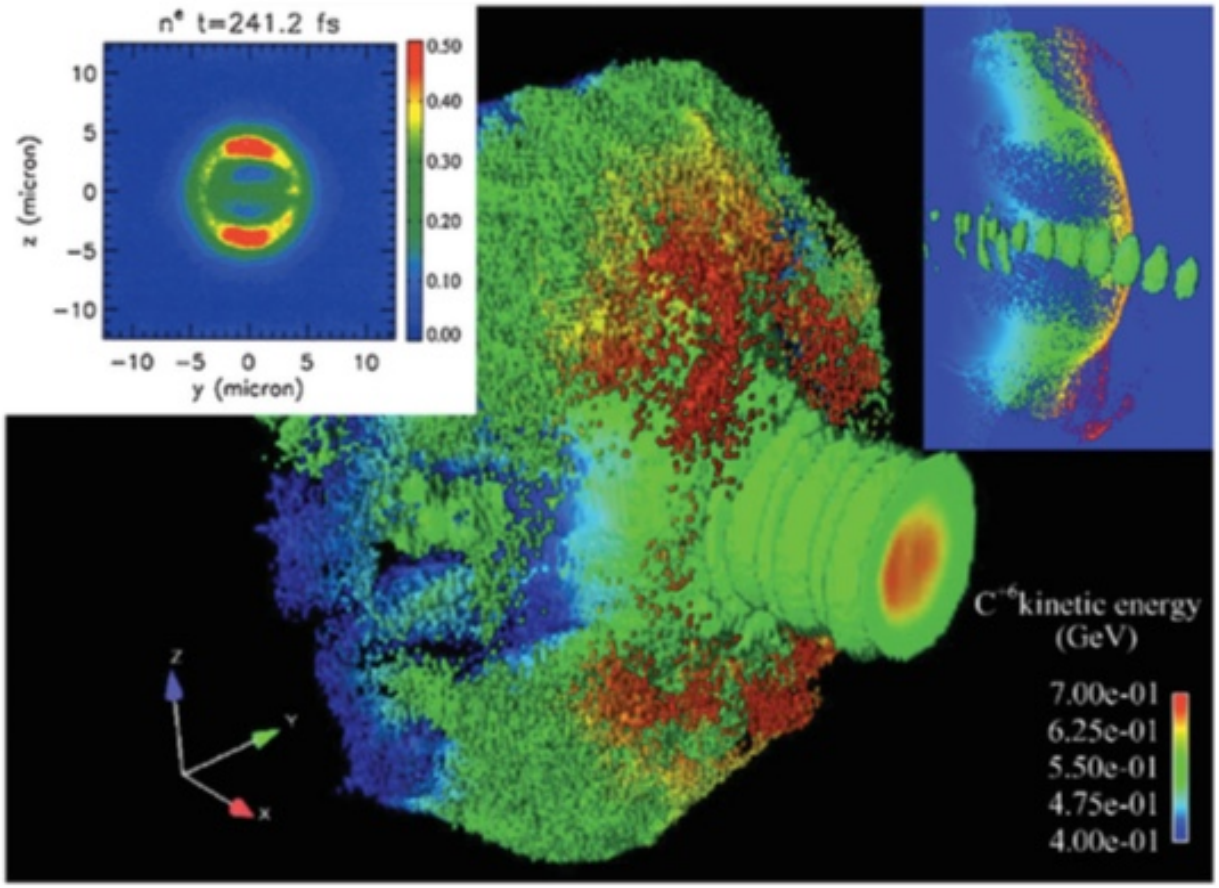

✓ Can enhance the maximum ion energies achieved c.f. TNSA

✗ Very thin targets difficult to handle

✗ Requires very small laser pre-pulse

✗ Asymmetric ion beam profile

L. Yin et al., Phys. Plasmas 14, 056706 (2007) ;
L Yin, et al, PRL, 107, 045003 (2011)

Advanced ion acceleration mechanisms: Magnetic vortex acceleration

SV Bulanov, et al, PRL, 98, 049503 (2007)

Azimuthal magnetic field associated with accelerated electron current

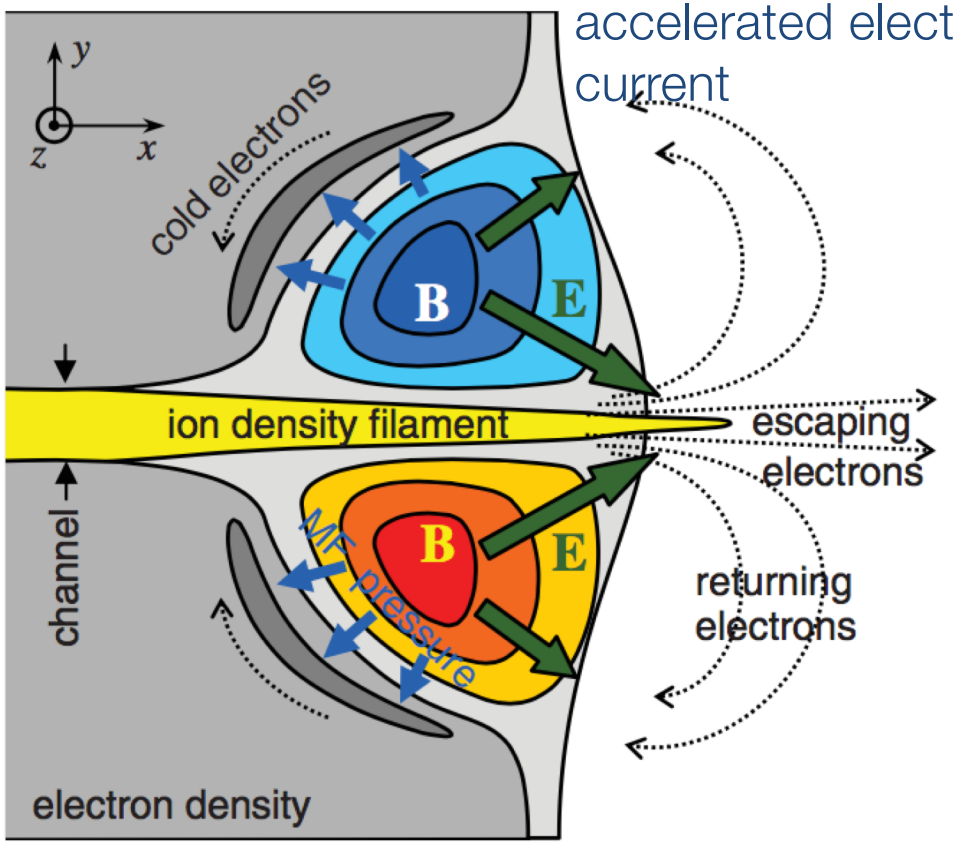

Magnetic pressure pushes back cold electrons, enhancing accelerating electric field

SS Bulanov, et al, Phys Plas, 17, 043105 (2010)

electrons

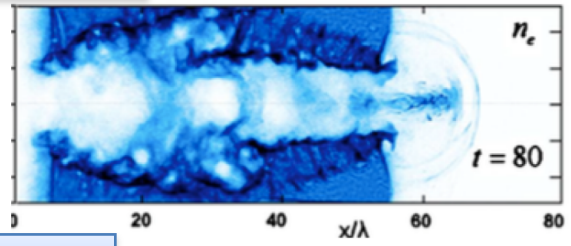

protons

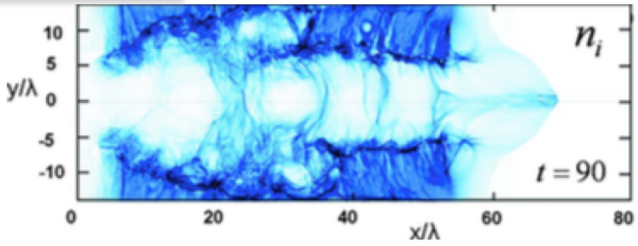

✓ Good ion energy scaling with laser intensity

✓ Good energy conversion efficiency

✗ Requires near-critical targets

✗ No conclusive experimental demonstrations yet

Advanced ion acceleration mechanisms: Shock acceleration

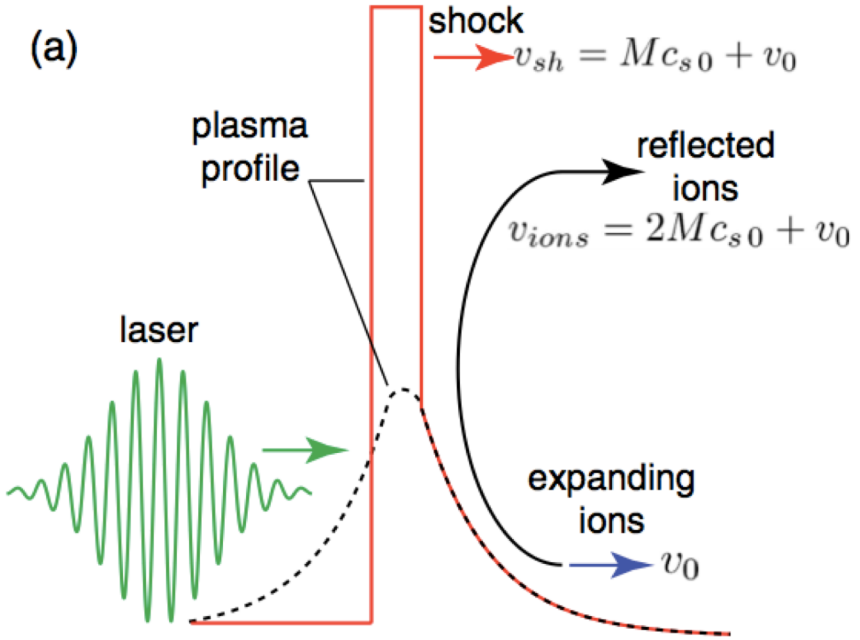

Very promising theoretical energy scaling with a_0:

a_0: 2.5, 5, 10, 15, 20

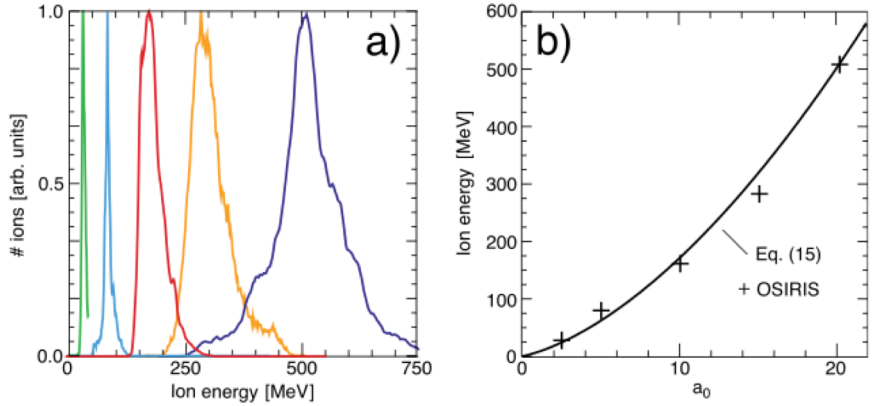

Demonstration of quasi-monoenergetic proton spectra using CO_2 (λ = 10 μm) lasers:

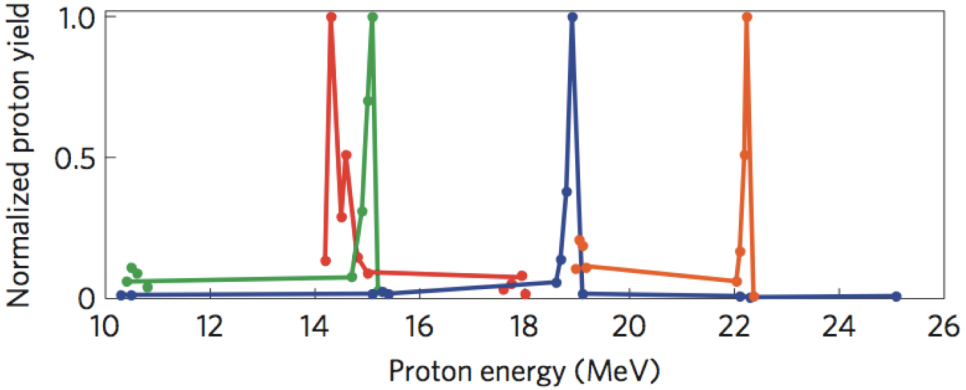

Laser	λ	n_c	a_0
CO_2	10 μm	10^{19} cm^{-3}	2
Glass	1.053 μm	10^{21} cm^{-3}	20
Ti:Sapph	800 nm	1.1×10^{21} cm^{-3}	50

D Haberberger, et al, Nature Physics, 8, 95 (2012);
F Fiuza, et al, PRL, 109, 215001 (2012);
F Fiuza, et al, Phys Plas, 20, 056304 (2013).

Advanced ion acceleration mechanisms: Shock acceleration

Shock formation requires a high plasma electron temperature, T_{e1}.

F Fiuza, et al, Phys Plas, 20, 056304 (2013)

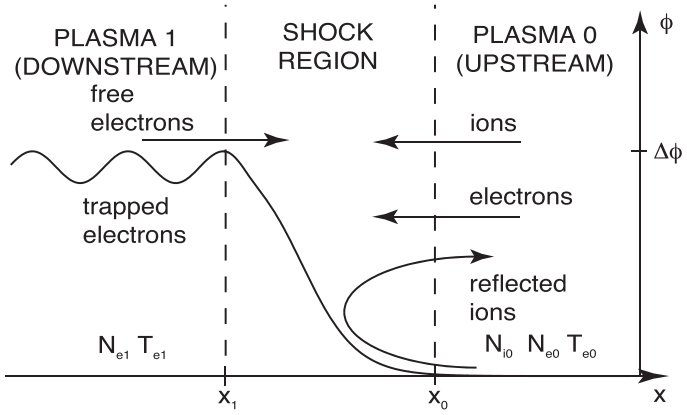

$$M_{cr} = \sqrt{2\frac{T_{e1}}{T_{e0}}\left(\frac{1+\mu_{e0}}{\frac{N_{e1}}{N_{e0}}\left(1-\mu_{e0}\frac{T_{e0}}{T_{e1}}\right)}+1\right)}$$

$$\mu_{e0} = \frac{m_e c^2}{k_B T_{e0}}$$

This requires strong laser absorption and places restrictions on the target size and scalelengths for optimum acceleration.

✓ Excellent ion energy scaling with laser intensity
✓ Quasi-monoenergetic acceleration
✓ Gas-jet useful for high-rep rate & low debris
✓ Experimentally demonstrated

✗ Requires challenging target parameters:
- Very-high density gas jet / prepared target
- Relativistic Transparency increases density requirement – even more difficult
- Carefully designed density profile needed

✗ Large focal spot needed, increases the laser energy required

✗ Instabilities not studied

Laser-driven Ion Acceleration Mechanisms: Common Physics Themes

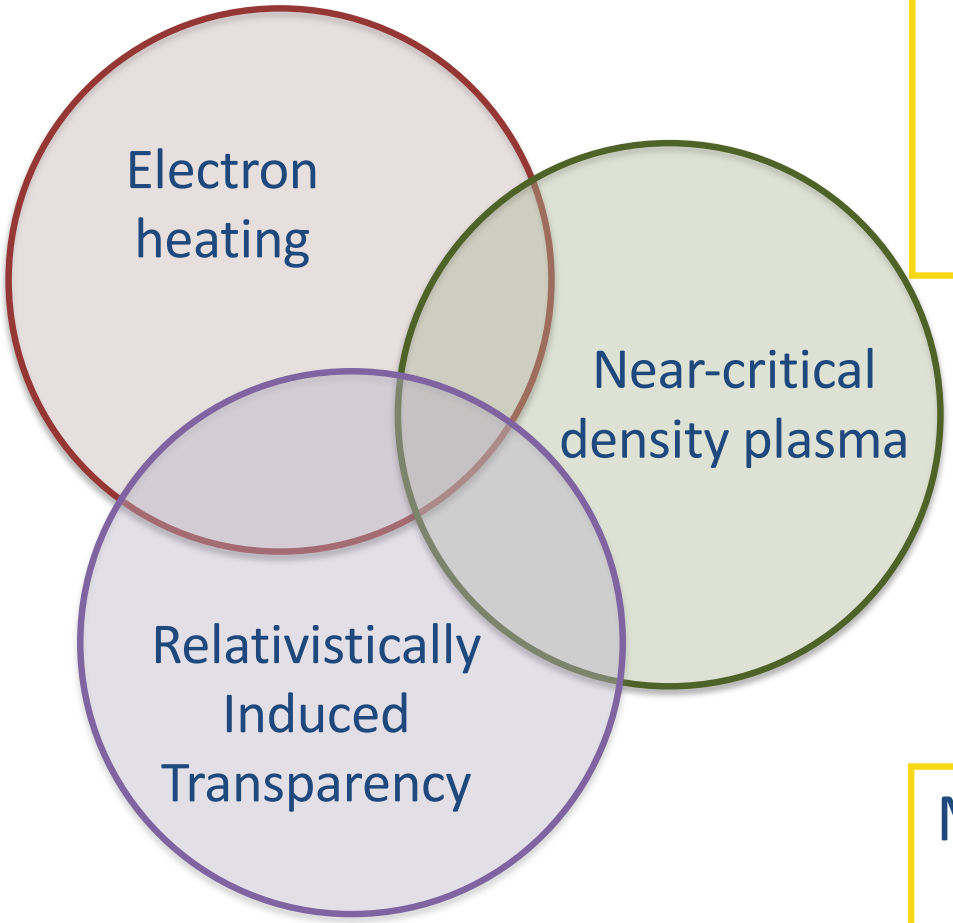

TNSA

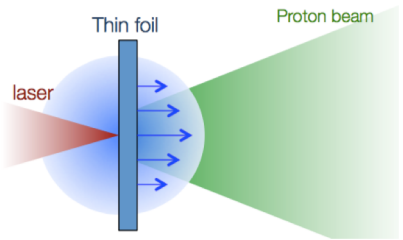

RPA

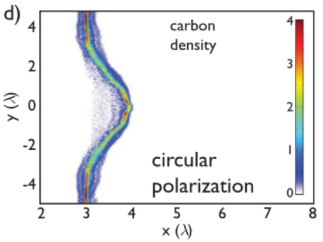

BOA

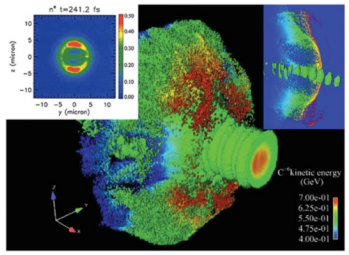

Magnetic vortex

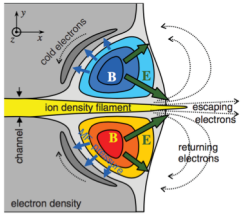

Shock

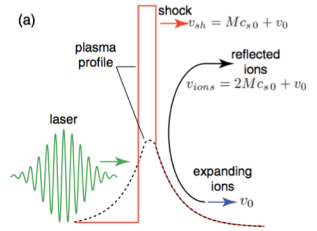

Other mechanisms:

- Ponderomotive pressure
- Directed Coulomb explosion

Overdense Plasma Interactions

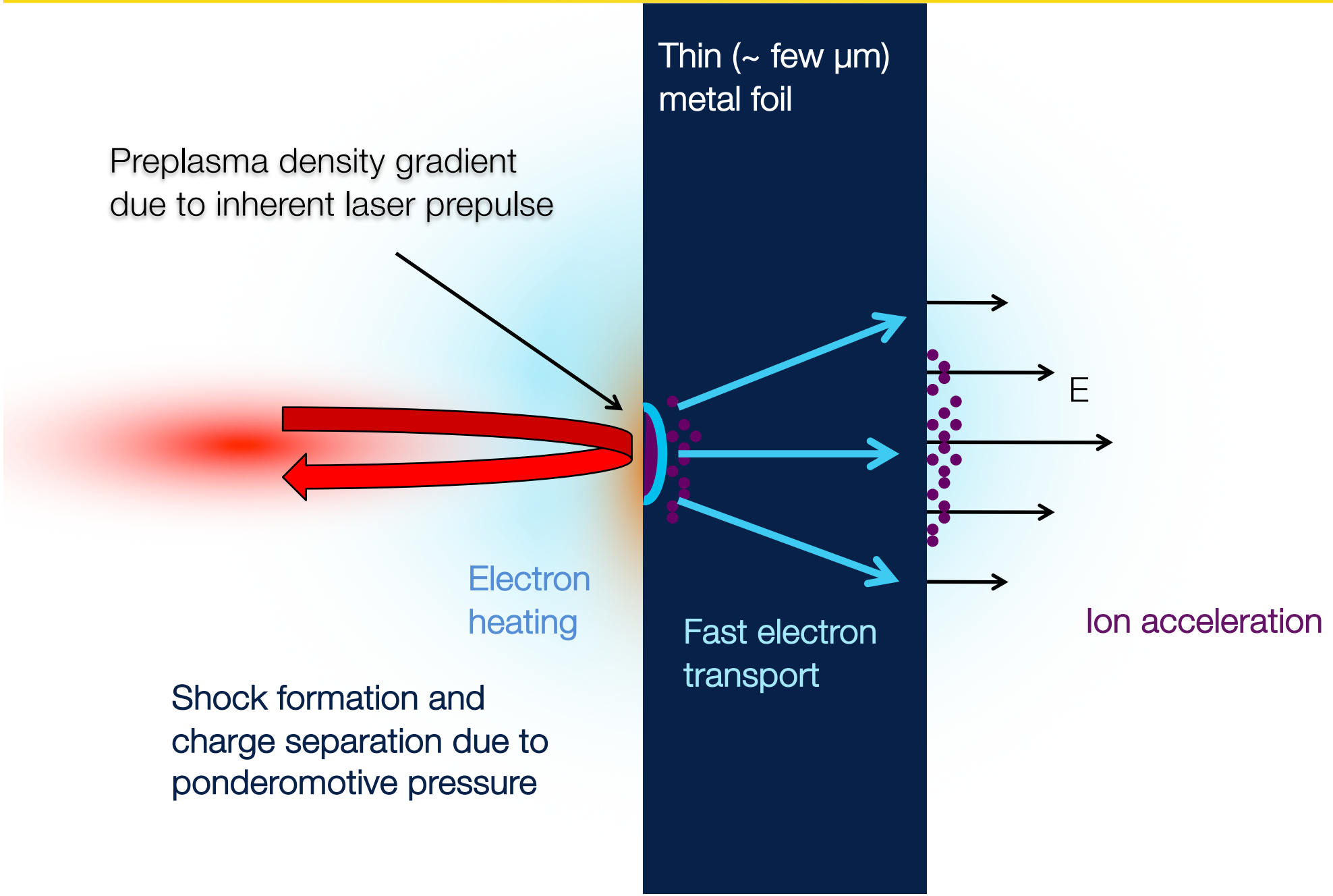

TNSA theory

1. Laser energy into hot-electrons
   - Pre-pulse conditions?
   - Hydrodynamic response of target to pre-pulse
   - PIC modeling of the interaction and electron heating
2. Hot electrons propagation through target
   - Hybrid PIC or fluid modeling needed
     - Effect of cold return current
     - Target resistivity
3. Ion expansion into the vacuum due to sheath electric field
   - PIC modeling
   - Analytic models

Theory approaches:

- Dynamic: ions and electrons expand into vacuum according to fluid model

S Wilks, et al., PoP, **8**,542 (2001);
P Mora, Phys. Rev. Lett., **90**, 185002 (2003)

- Quasi-static electric field: Hot electrons set up electric field and ions are test particles

J Schreiber,et al., PRL, **97**, 045005 (2006);
M Passoni & M Lontano, Phys. Rev. Lett., **101**, 115501 (2008)

TNSA: initial electric field

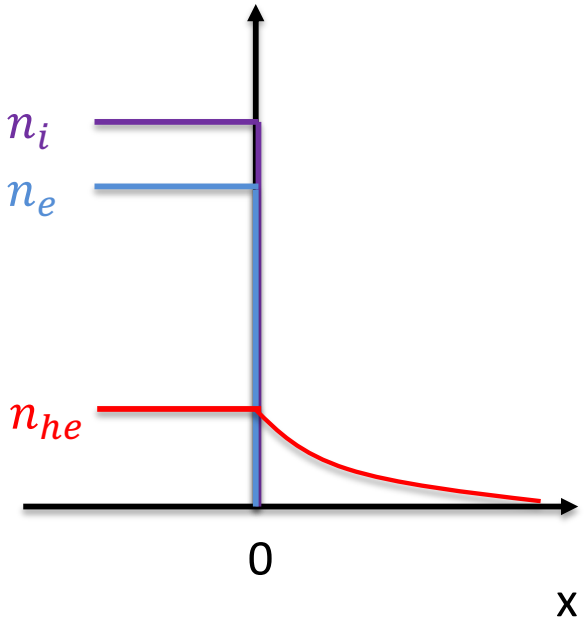

At the rear, $n_{he} = n_0 \exp\left(-\frac{x}{\lambda_D}\right)$

Charge density, $\rho = -en_{he} = -en_0 \exp\left(-\frac{x}{\lambda_D}\right)$

Gauss's law: $\nabla . \bar{E} = \frac{\overline{dE}}{dx} = \frac{\rho}{\varepsilon_0}$

So at the rear surface, $x = 0$

$$E(0) = \int_0^\infty \frac{\rho}{\varepsilon_0} dx = \frac{en_0\lambda_D}{\varepsilon_0} = \frac{en_0}{\varepsilon_0}\sqrt{\frac{\varepsilon_0 k_B T_e}{n_0 e^2}}$$

$$= \frac{k_B T_e}{e}\sqrt{\frac{n_0 e^2}{\varepsilon_0 k_B T_e}}$$

$$E(0) = \frac{k_B T_e}{e\lambda_D}$$

Need to know the initial rear surface electron density, n_0, and temperature, T_e, for the hot electrons

TNSA models: Mora model

P Mora, Phys. Rev. Lett., **90**, 185002 (2003)

Dynamic model: ion expansion modifies the electric field, $\bar{\bar{E}}(t)$

Expansion has self-similar solutions (depend only on x and t)

$$u_i = c_s + \frac{x_i}{t}$$

$$n_i = n_{i0} \exp\left[-\left(1 + \frac{x_i}{c_s t}\right)\right]$$

Where the ion sound speed $c_s = \sqrt{Z k_B T_e / m_i}$

But this isothermal model implies infinite acceleration so some limit has to be imposed…

Solutions become invalid when the local Debye length

$$\lambda_D = \lambda_{D0}\sqrt{n_{e0}/n_e} = \lambda_{D0} \exp\left[\frac{1}{2}\left(1 + \frac{x_i}{c_s t}\right)\right]$$

equals the density scalelength, $c_s t$

Predicts the ion front position and velocity and implies the electric field at the ion front is twice that predicted by the self-similar solution.

TNSA models: Mora model

P Mora, Phys. Rev. Lett., **90**, 185002 (2003)

Mora developed a 1D Lagrangian code to more accurately determine the electric field at the ion front over time.

$$E_{front} = \sqrt{\frac{2}{e_E}}\frac{E_0}{\sqrt{1+\tau^2}}$$

Where $\tau = \omega_{pi}t/\sqrt{2e_E}$ is the acceleration time $\quad e_E = 2.718\ldots$

From this you can find the ion front velocity

$$v_{front} \approx 2c_s \ln\left(\tau + \sqrt{\tau^2+1}\right)$$

Can assume the acceleration time is the same as the fast electron time or the laser pulse duration, τ_L

Get well defined cutoff energy

$$\varepsilon_{max} = \tfrac{1}{2}m_i v_{front}^2 \approx 2Zk_BT_e\left[\ln\left(\tau + \sqrt{\tau^2+1}\right)\right]^2$$

Also predicts the spectral shape

$$\frac{dN}{d\varepsilon_i} = \frac{n_{i0}}{\sqrt{2\varepsilon_i}}\exp\left(-\sqrt{\frac{2\varepsilon_i}{Zk_BT_e}}\right)$$

Relativistic intensity electron heating mechanisms: Soild target, steep density gradient

How is the laser energy transferred to the electrons at relativistic intensities?

overdense, sharp density gradient

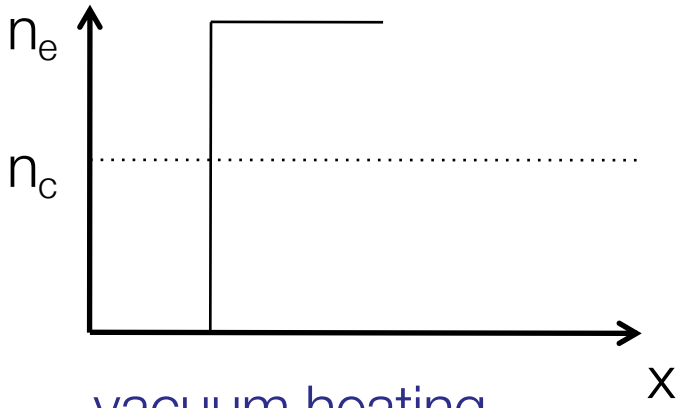

vacuum heating
or j x B heating

$$T_e \propto U_p \approx (a_0/2)^2 m_e c^2$$

S C Wilks, et al, PRL, 69, 1383 (1992)

Vacuum heating

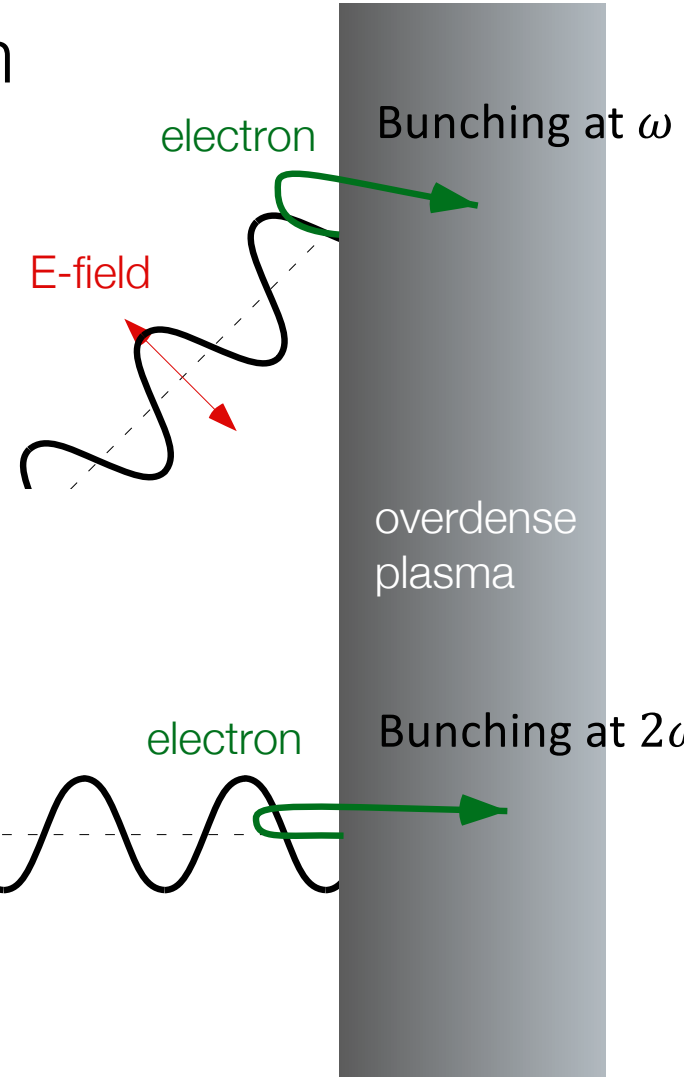

Relativistic intensity electron heating mechanisms: Temperature of the hot electrons

M Haines, et al, PRL, 102, 045008 (2009)

- Up to intensities of ~10^{19} Wcm^{-2}, T_e agreed well with ponderomotive theory
- Beg's law is a fit to experimental data

$$T_e = 215\left(I_{18}\lambda_{\mu m}^2\right)^{1/3}$$

FN Beg et al., Phys. Plasmas 4, 447 (1997)

- Haines's relativistic model gets close to Beg's scaling

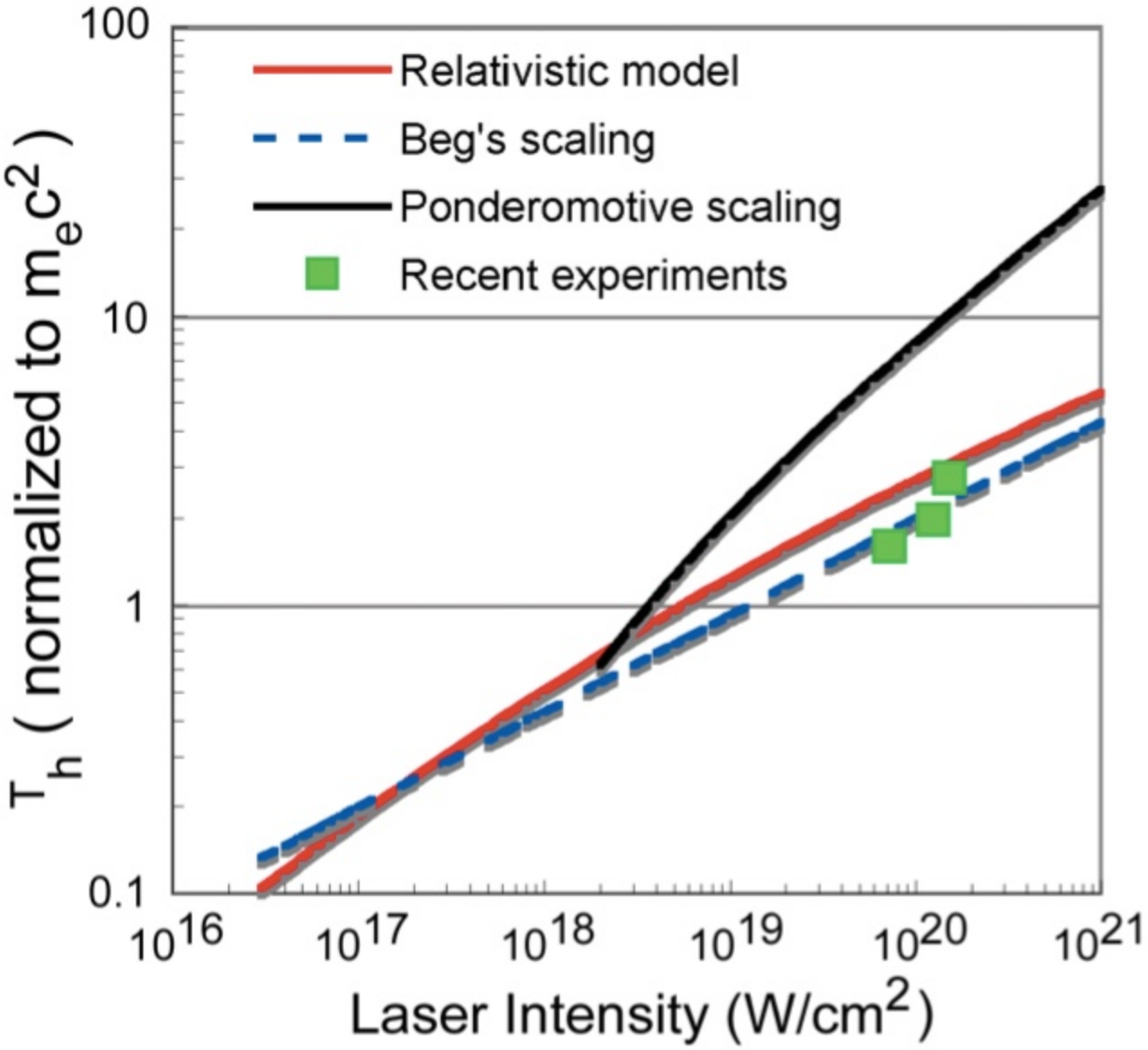

Relativistic intensity electron heating mechanisms: Total energy into hot electrons

- Absorption of laser energy into the plasma has been measured to be up to 80-90% in the ultra-relativistic regime,
  $I > 10^{20}$ Wcm^{-2}.

- Usually the absorption is found to be closer to 30% for most experimental conditions.

Y Ping, et al, PRL, 100, 085004 (2006)

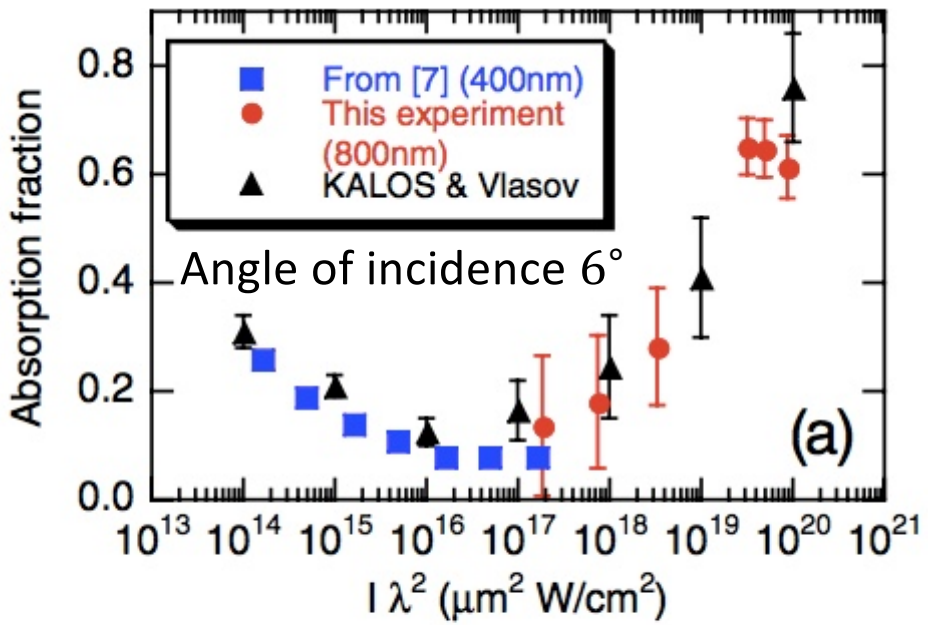

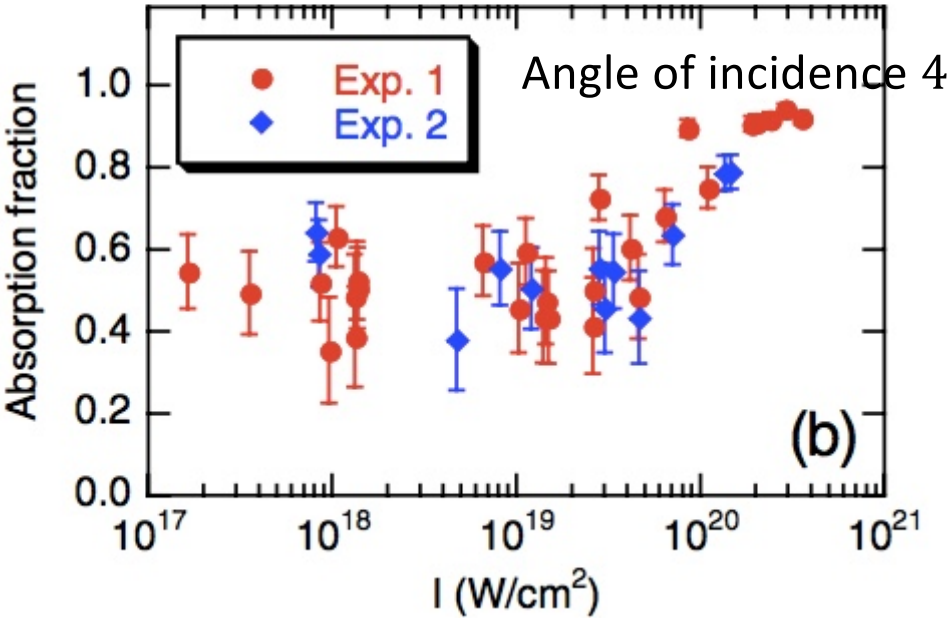

Relativistic intensity electron heating mechanisms: Initial electron beam divergence

As the intensity increases, electron beam divergence seems to increase

JS Green et al, PRL, **100**, 015003 (2008)

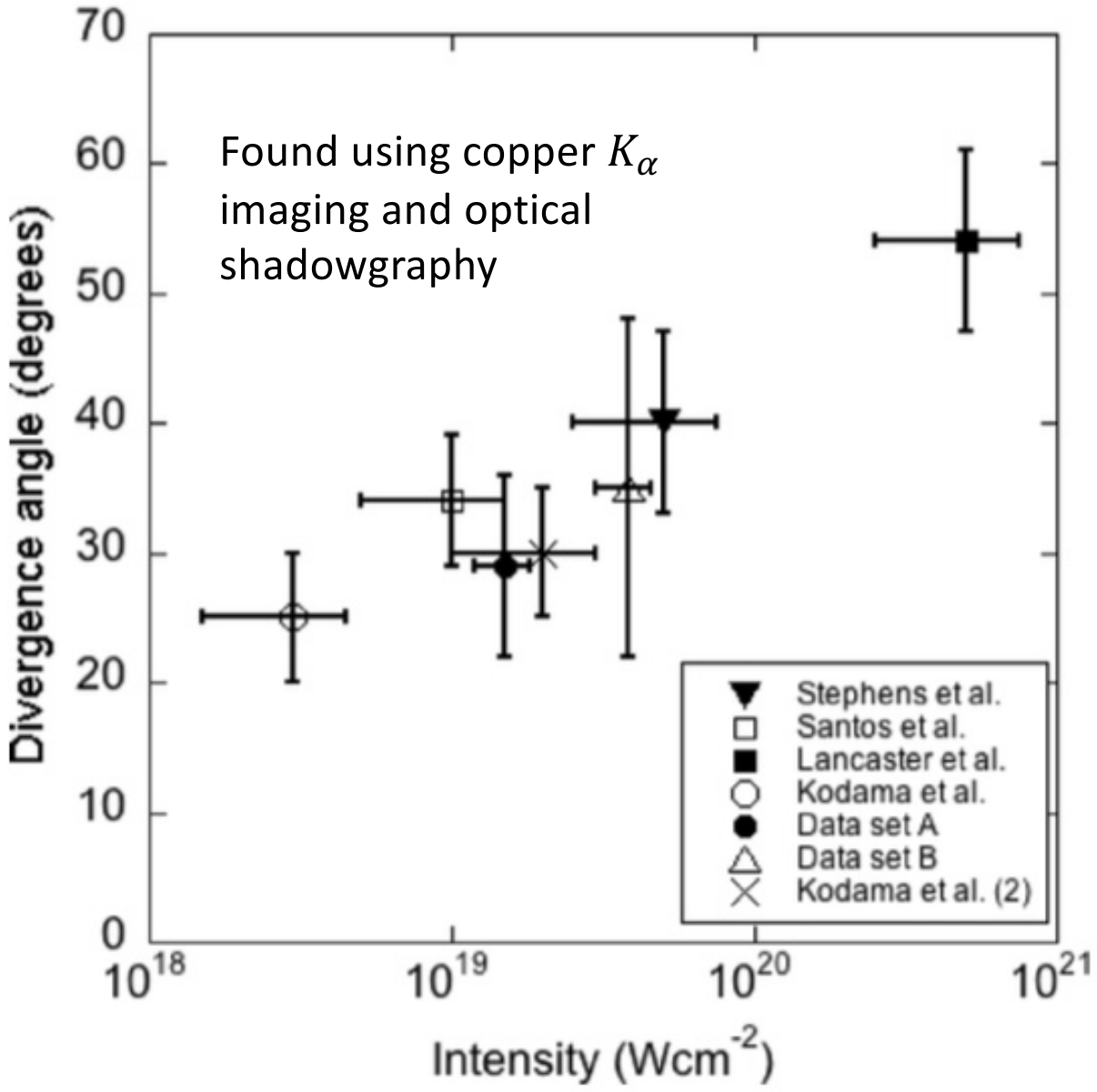

Fast electron transport

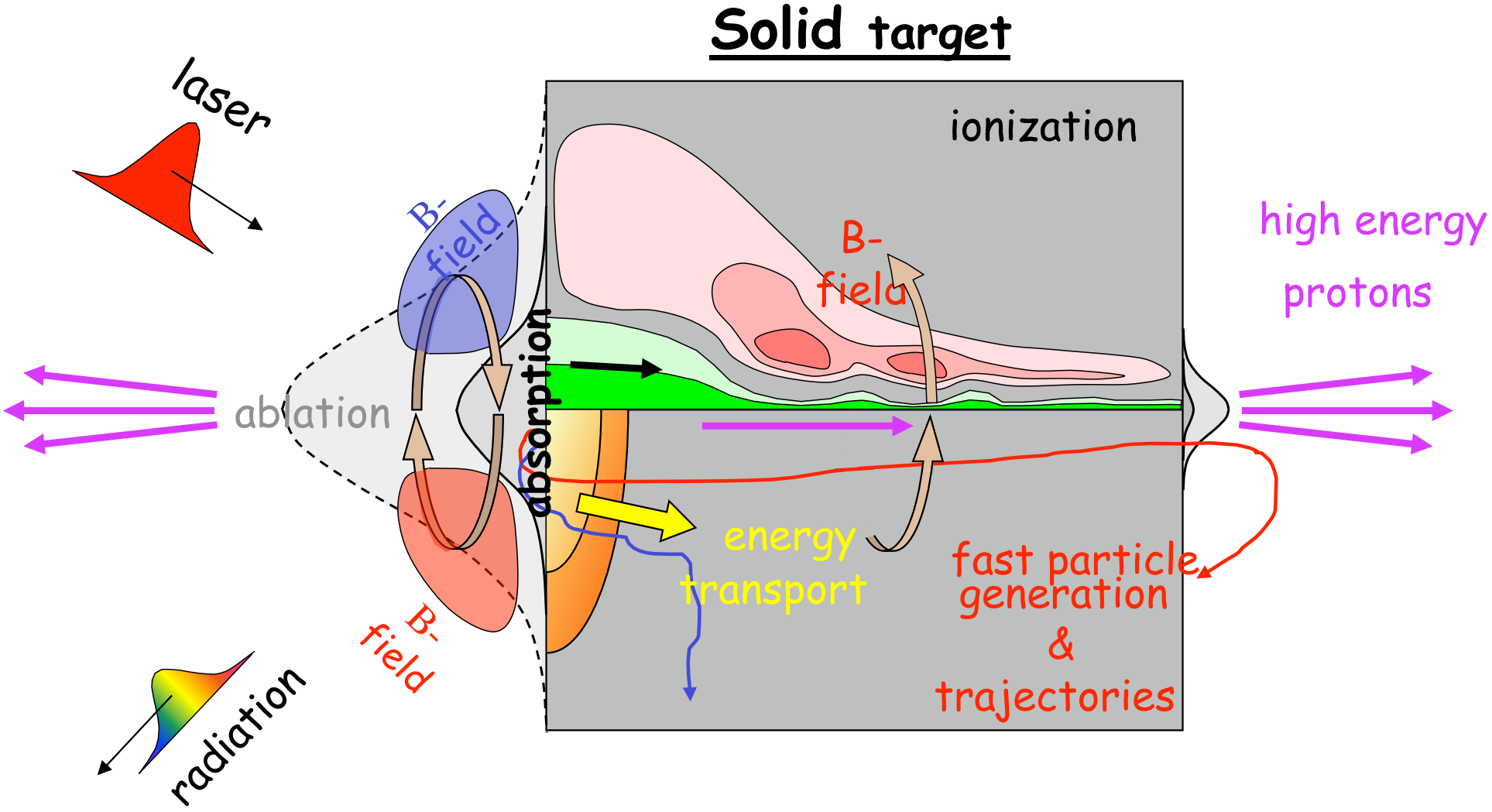

Fast electron transport

- The hot electron beam has high current, which creates a huge magnetic field to collimate the beam. It was initially thought the high current would heat the material to create a high conductivity path.
- **Alfvén current,** I_A, is the maximum current that can propagate in a vacuum:

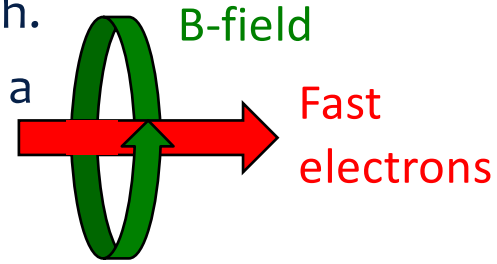

$$I_A = \frac{m_e c^3}{e}\beta\gamma = 17\beta\gamma\left[kA\right] \qquad \text{where } \beta = v_e / c$$

Above this limit the self-consistent azimuthal magnetic field around the current is too large to allow the current propagation and turns the electrons back on themselves through the $\boldsymbol{v}$ x $\boldsymbol{B}$ force.

- However, the hot electron beam is created by a laser interaction within a neutralized material. Therefore accelerating a hot electron current, j_{fast}, into the material will leave the target charged at the production site. A return current, j_{cold}, will be drawn from the cold background electrons to correct the imbalance.
- The return current reduces the magnetic field and allows fast electron currents greater than I_A to propagate.

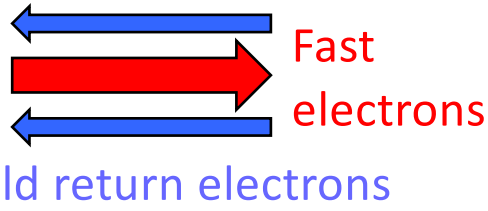

Fast electron transport: Weibel instability

- The interaction of fields generated by the counter propagating currents, j_{fast} and $j_{cold,}$ gives rise to the electromagnetic **Weibel instability**
- This causes the electron beam to break up and filament into individual electron beams with transverse dimensions on the order of the collisionless skin depth, c/ω_{pe}.
- Each individual filament can carry, I_A, so the total current can exceed the Alfvén limit.

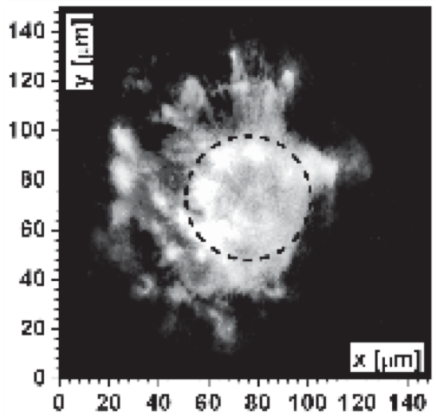

FIG. 3. Optical emission data obtained using a 250 μm foam target. The image shows the reprocessed data obtained from both cameras with different gray filters by overlying in order to show the substructure of the inner circle as well as the filaments in the outer region. The positions of the inner filaments are indicated with a circle with 50 μm in diameter, whereas the spot including the filaments in the outer region has a diameter up to 100 μm.

R. Jung et al., Phys. Rev. Lett., **94**, 195001 (2005)

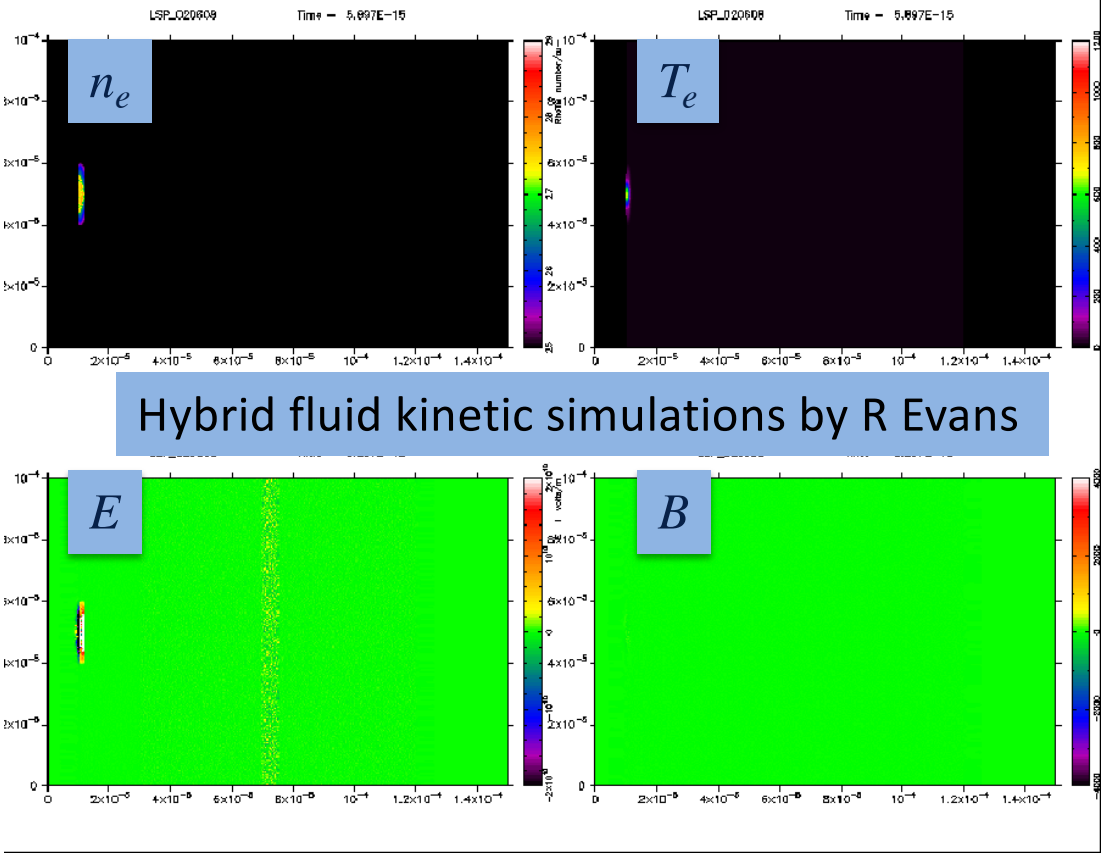

Fast electron transport: Affects proton beam properties

P McKenna, et al., PRL, 106, 185004 (2011)

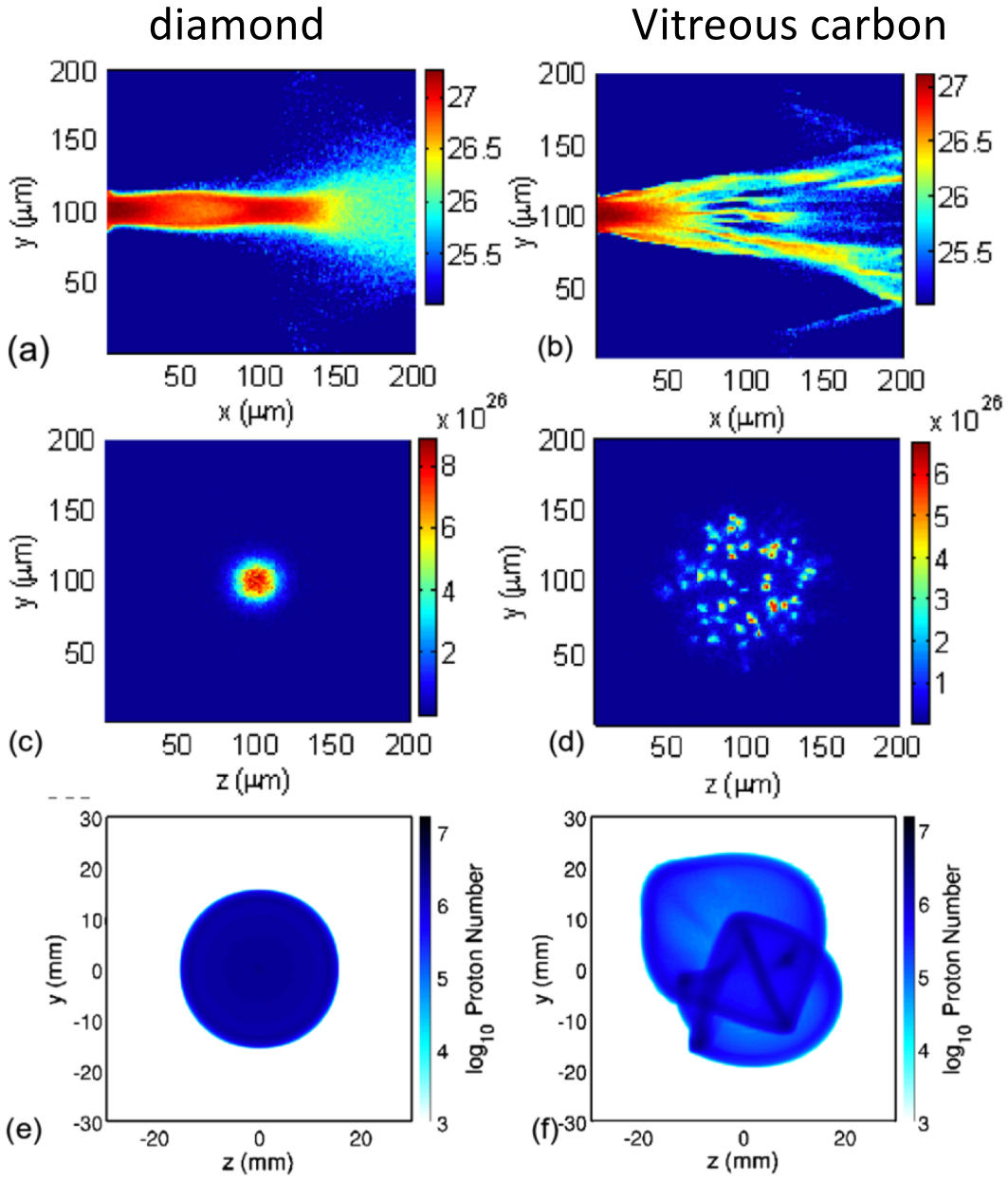

Hot electron structures on the rear side of the target can affect the proton beam structure

Rear side hot electron density

Simulated proton beam profile

Proton and ion diagnostics: Energy spectra
Thomson Parabola Spectrometer

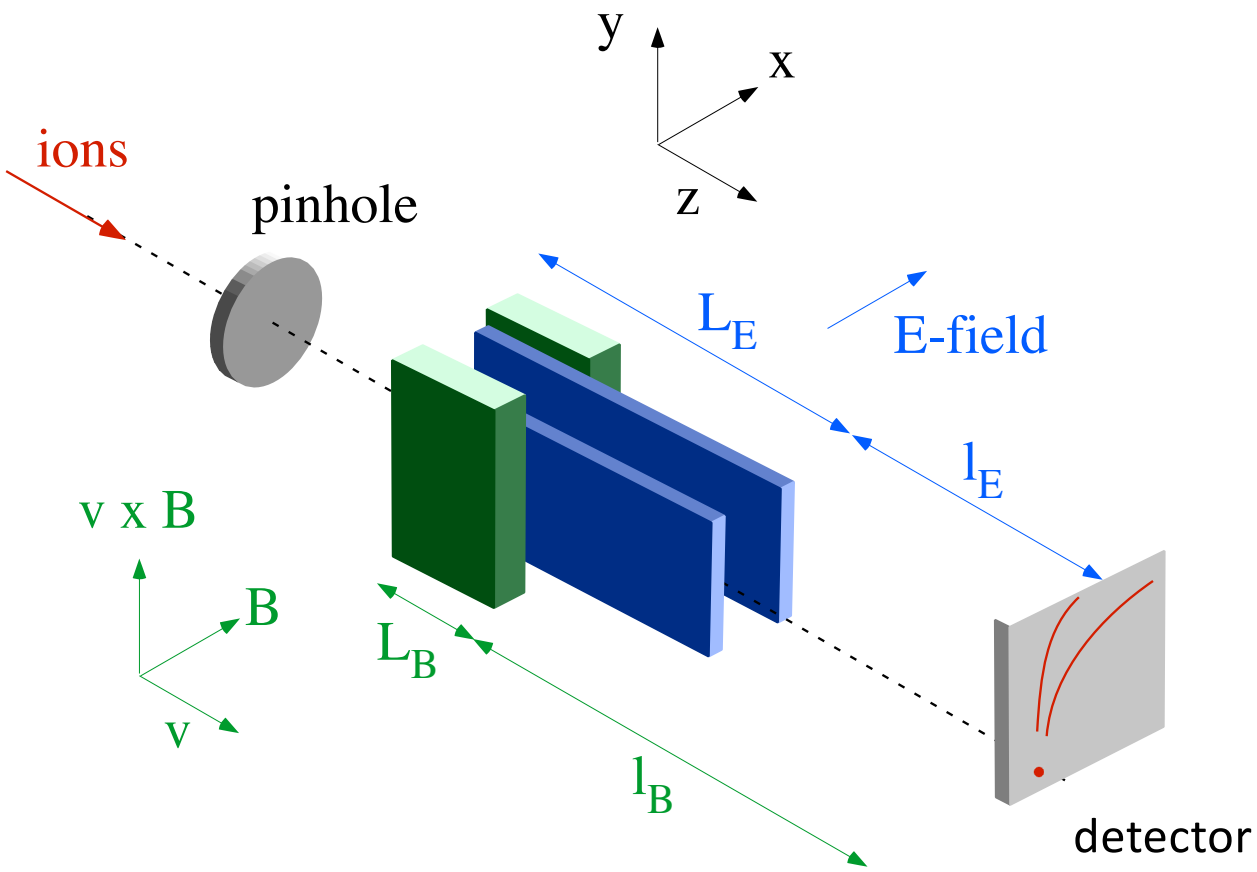

From the Lorentz force,

$$\underline{F} = Ze\left(\underline{E} + \underline{v}\times\underline{B}\right)$$

and using small angle approximations, it can be shown that the deflection at the detection plane is given by:

$$x = \frac{ZeEL_E}{Av^2m_u}\left[\frac{L_E}{2} + l_E\right]$$

$$y = \frac{ZeBL_B}{Avm_u}\left[\frac{L_B}{2} + l_B\right]$$

where m_u is the 1/12 mass of ^{12}C, A is the atomic mass number and Z is the charge on the ion.

Eliminating v gives a unique parabola on the detector for a given charge-to-mass ratio:

$$y^2 = \frac{ZeB^2L_B^2}{Am_uEL_E}\left[\frac{L_B}{2} + l_B\right]^2\left[\frac{L_E}{2} + l_E\right]^{-1}x$$

Proton and ion diagnostics: Energy spectra
Thomson Parabola Spectrometer

Assuming v << c, the kinetic energy of the ion, $E_{ion} = \frac{1}{2}Am_u v^2$, is therefore:

$$E_{ion} = \frac{\left[ZeBL_B\left(\frac{1}{2}L_B + l_B\right)\right]^2}{2Am_u}\frac{1}{y^2}$$

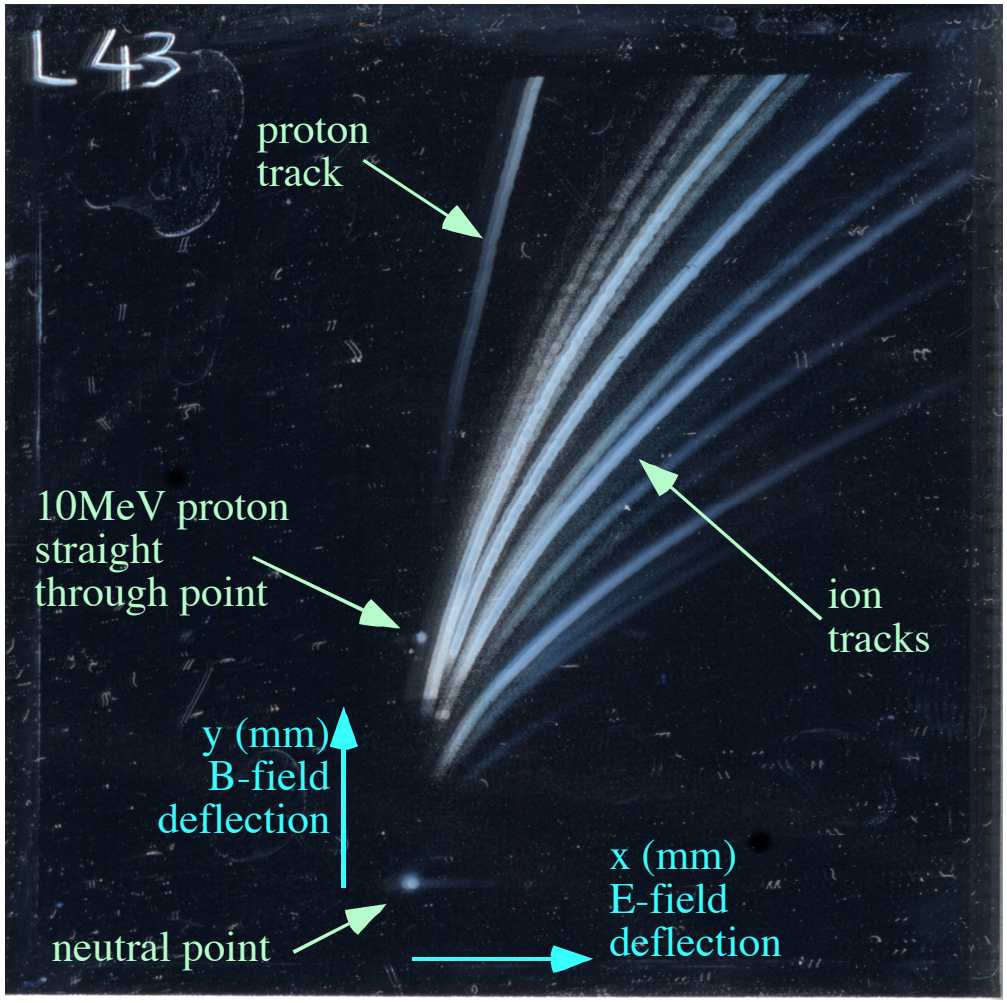

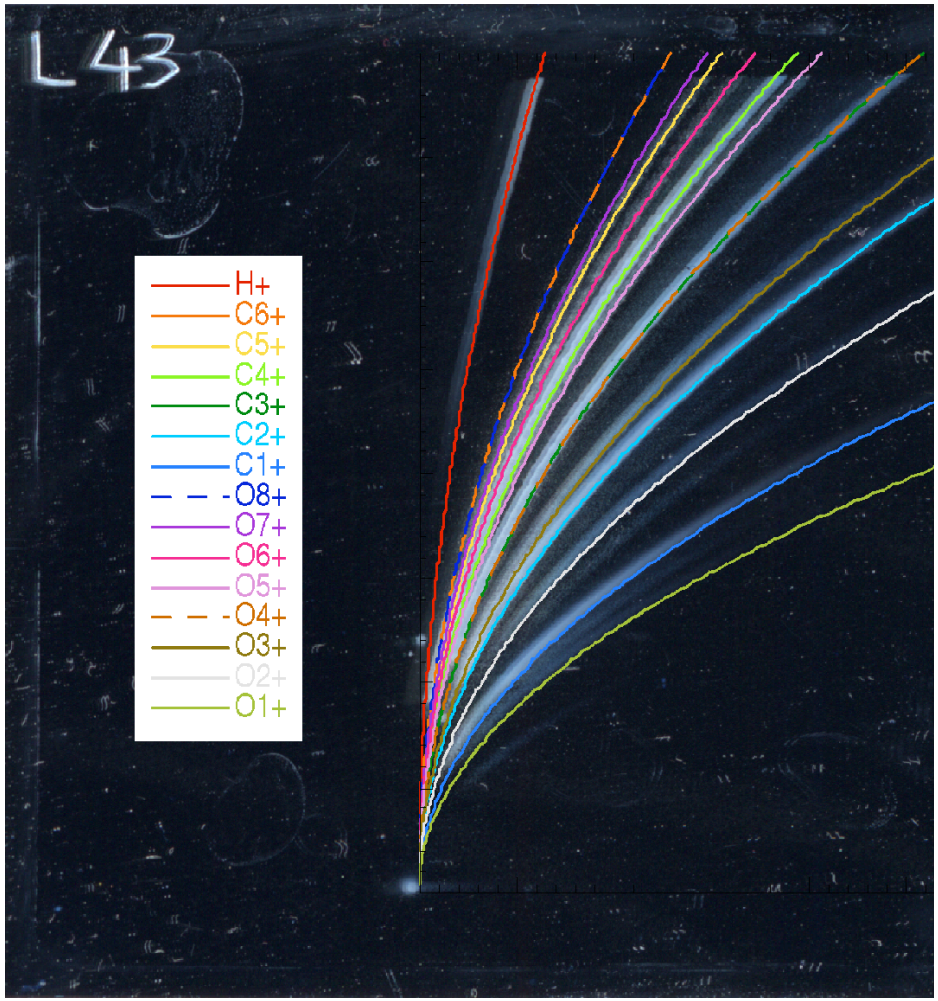

Proton and ion diagnostics: Proton stopping power in materials

The stopping power of a material, dE/dx has contributions from the electronic and nuclear interactions.

At low proton energy, the electronic component reaches a maximum – this is known as the Bragg peak.

The proton/ion suddenly deposits a large amount of energy in a small volume – see energy loss vs distance example plot.

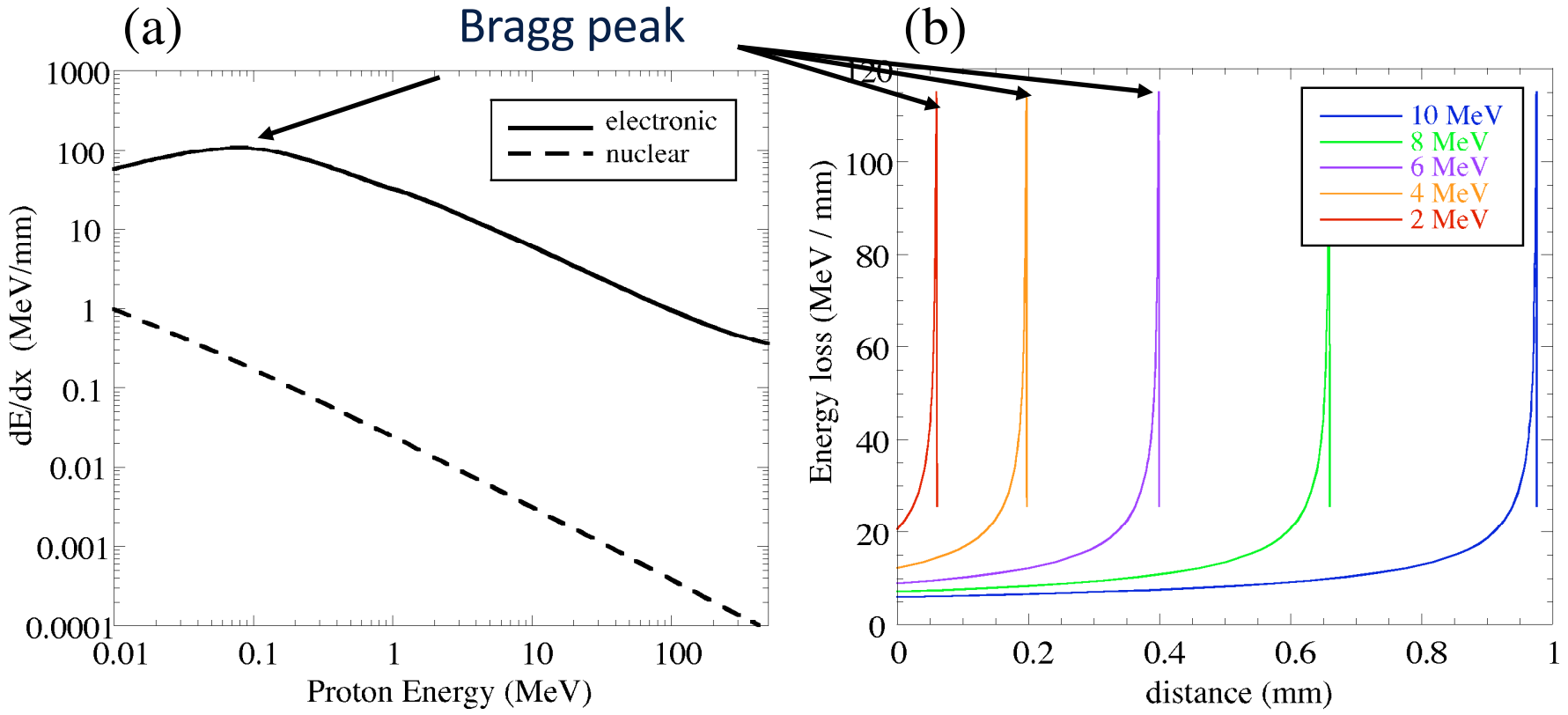

Proton and ion diagnostics: CR39 detector

- To expose damaged regions, CR39 is etched in a warm (~ 85° C) bath of 20% concentrated sodium hydroxide (NaOH) solution
- Damaged regions dissolve faster producing an etched pit for each stopped ion
- Pits can be inspected and counted using a microscope
- Pit size depends on:
  - Depth ion stopped at (i.e. initial energy)
  - Temperature of NaOH
  - Etching time
- Detection efficiency can be ~100%

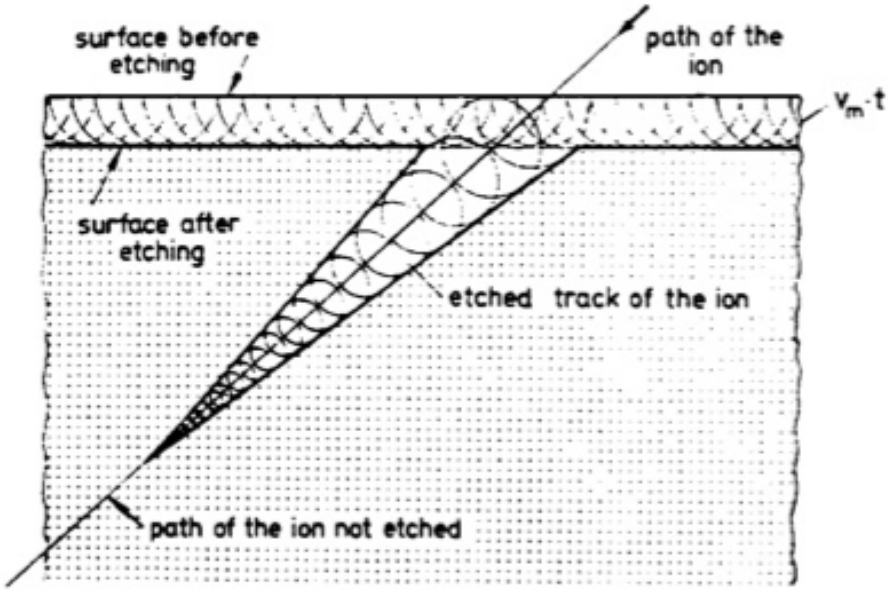

Fig. 1. Side view of an etched track. Huygens' principal is applied to describe etch cones of charged particles (Enge,1980).

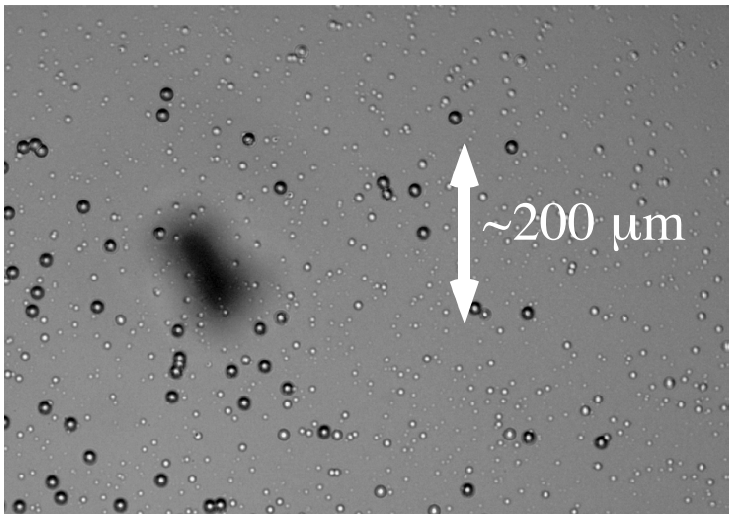

Proton and ion diagnostics: Radiochromic film (RCF)

- Thin polyester substrate films containing active layer of dye – triphenyl methane dye cyanide
- Insensitive to optical light
- Ionizing radiation induces a photo-chemical reaction – film goes from transparent to blue
- Optical density is proportional to radiation dose
- Sensitivity depends on film type

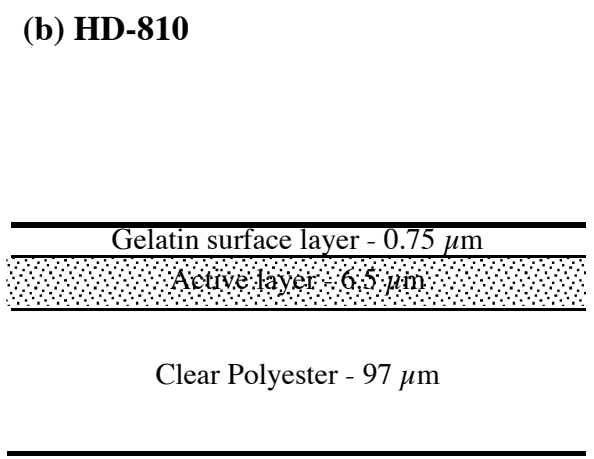

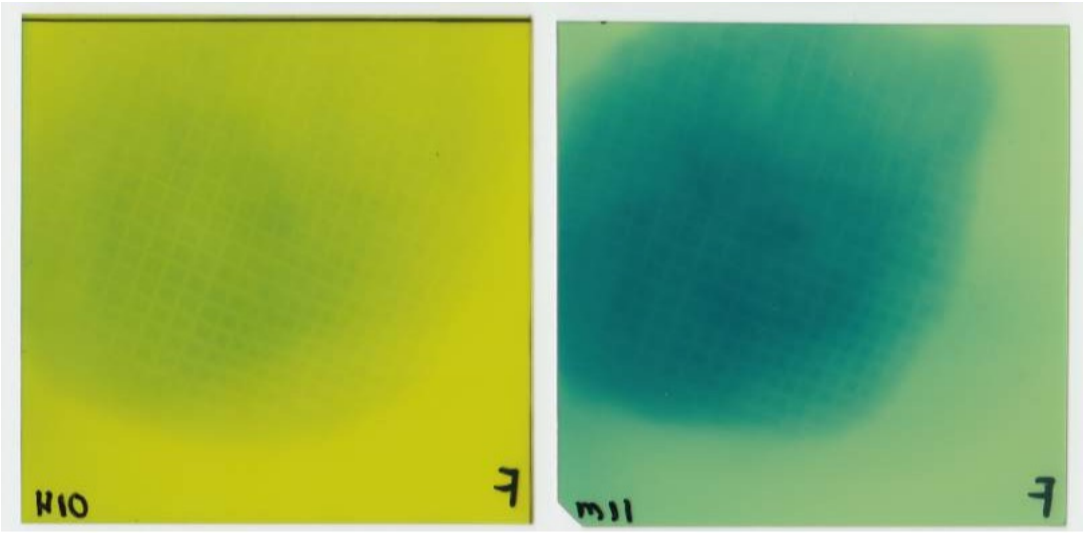

Proton and ion diagnostics: Radiochromic film (RCF) stacks

DS Hey, et al, Review of Scientific Instruments, 79, 053501 (2008)

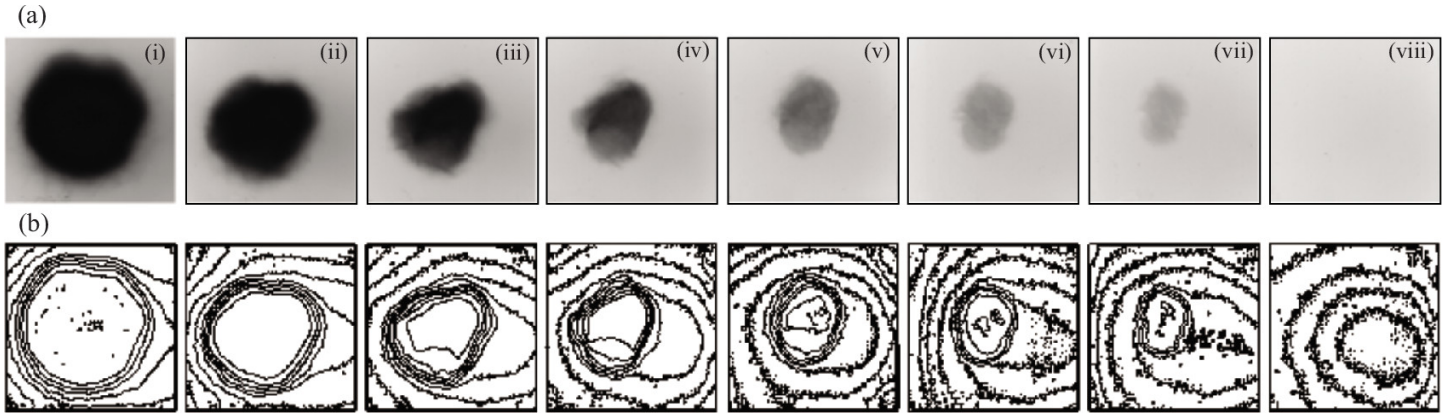

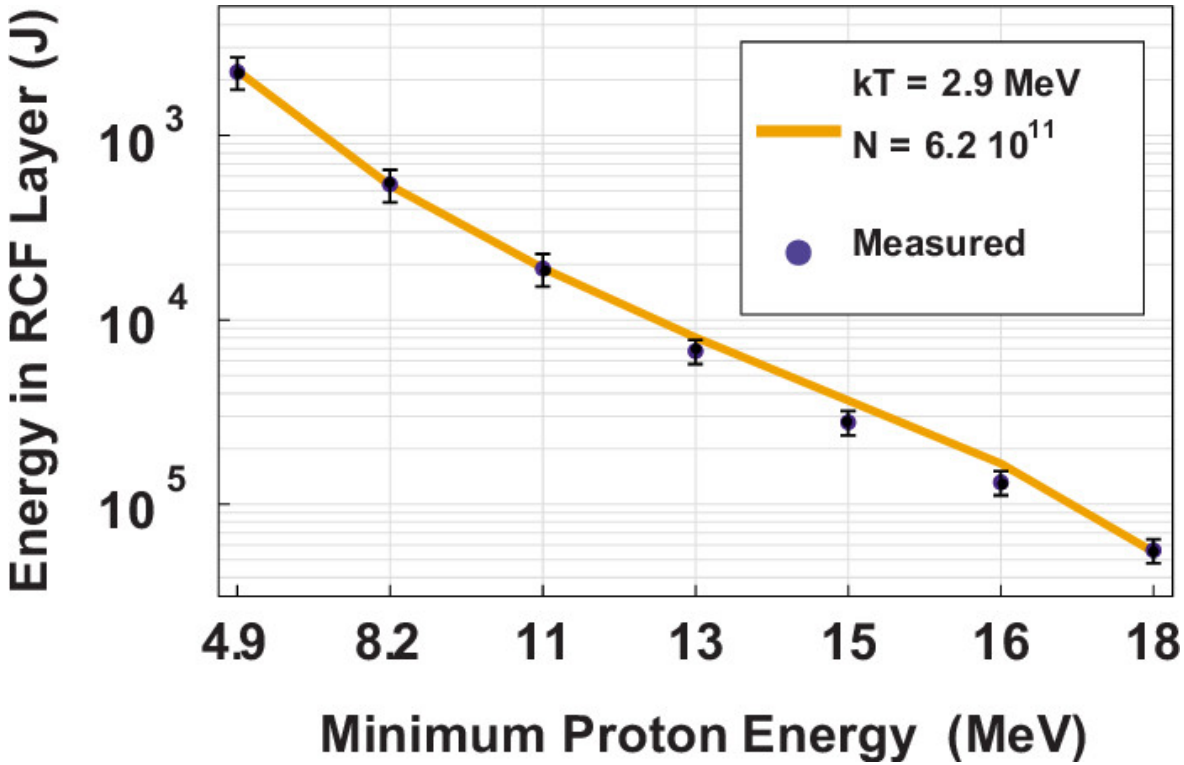

Reconstruct the proton spectra by subtracting higher energy contributions from the dose of each layer…

TNSA proton beam properties: Energy spectrum

RA Snavely, et al, PRL, 85, 2945 (2000)

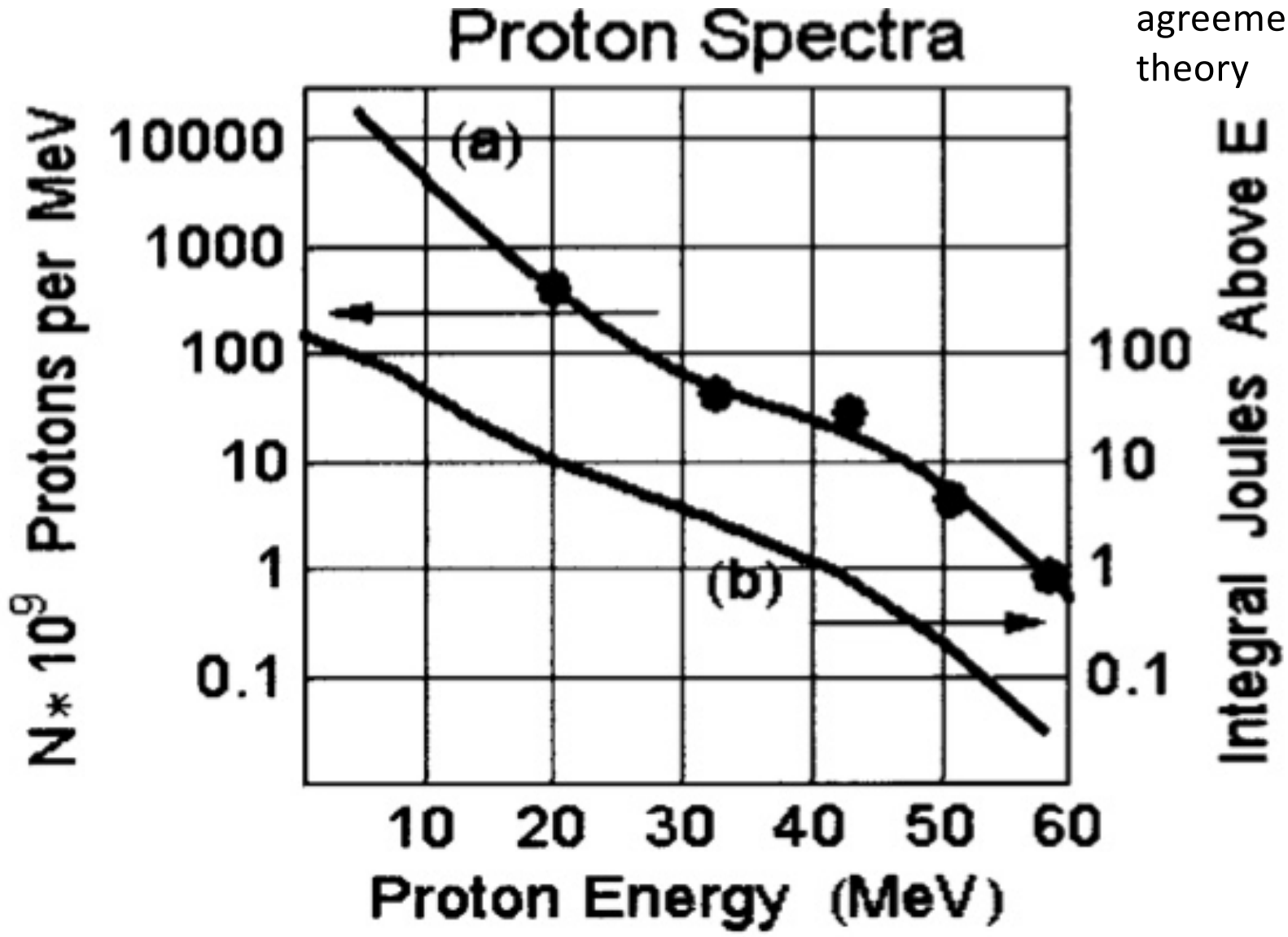

Quasi-Maxwellian – in agreement with Mora theory

TNSA proton beam properties: Maximum proton energy

J Fuchs, et al, Nature Physics, 2, 48 (2006)

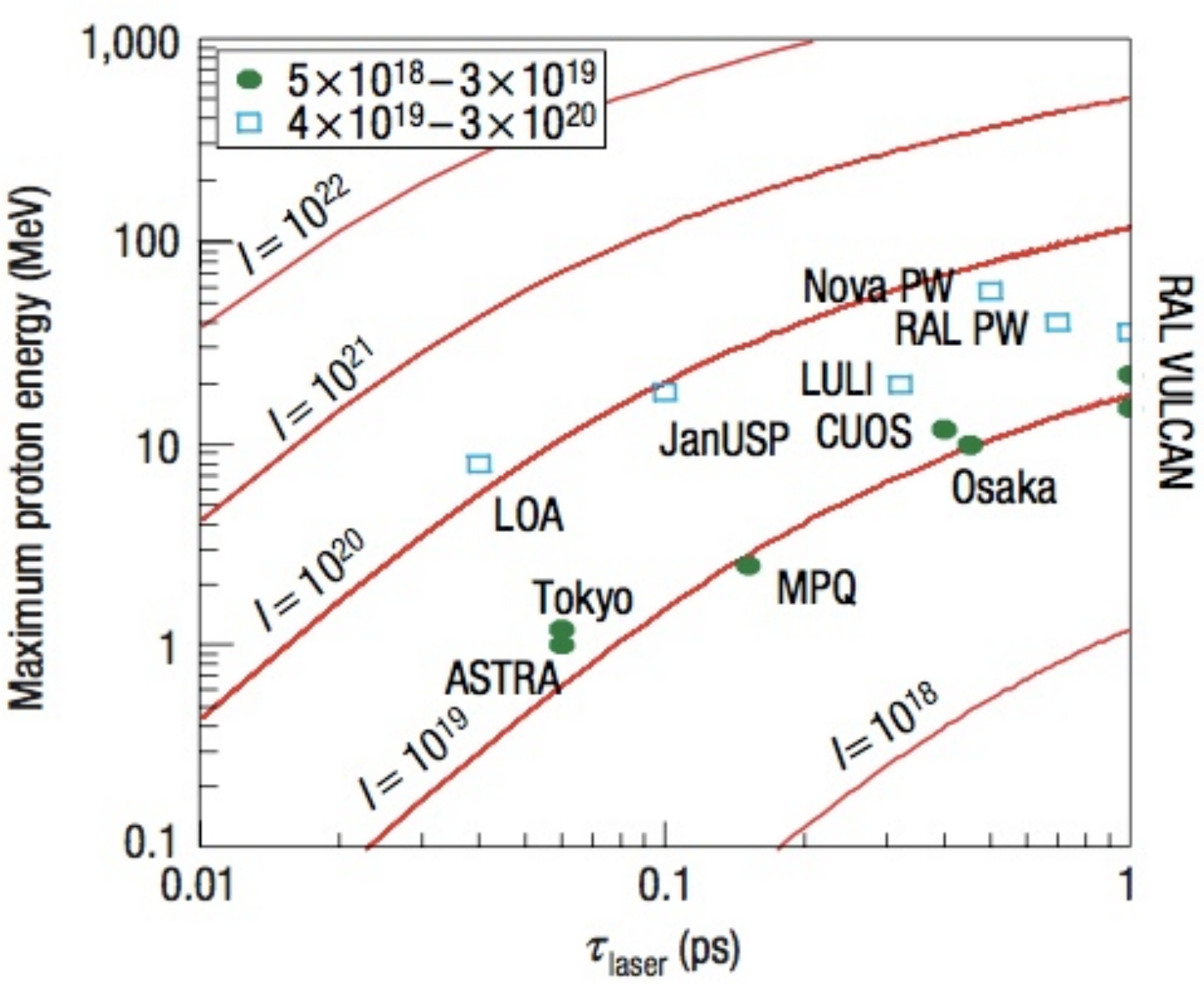

Intensity contours show predictions from a fluid model, similar to Mora with the acceleration time $\tau_{acc} = 1.3\tau_L$

TNSA proton beam properties: Transverse emittance

TE Cowan, et al., PRL, 92, 204801 (2004)

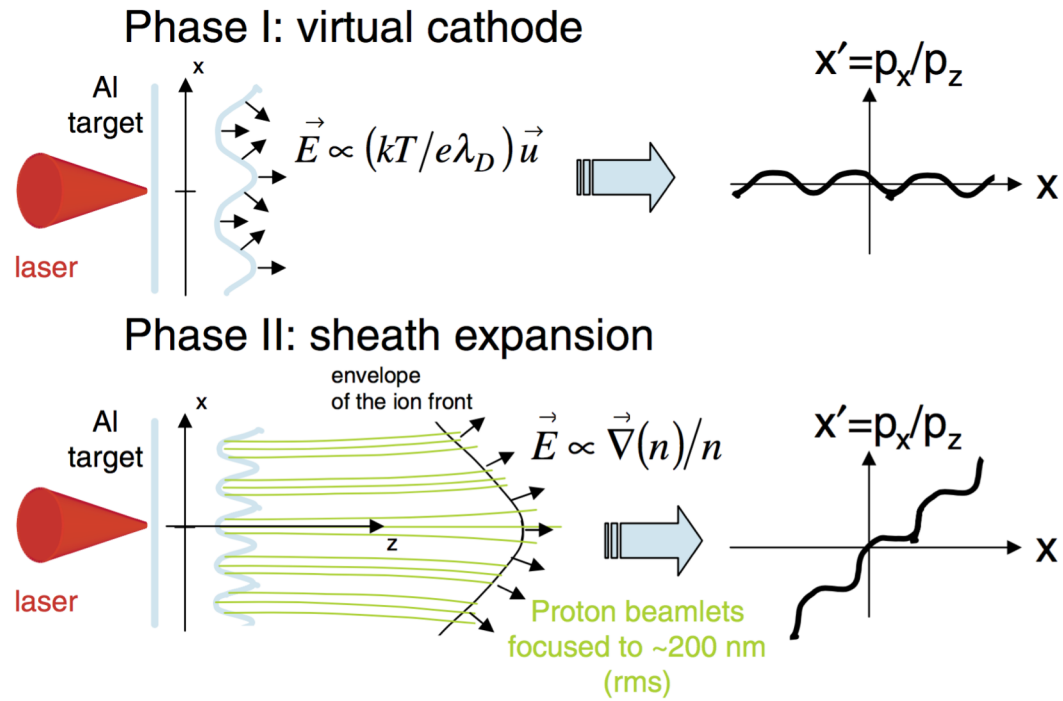

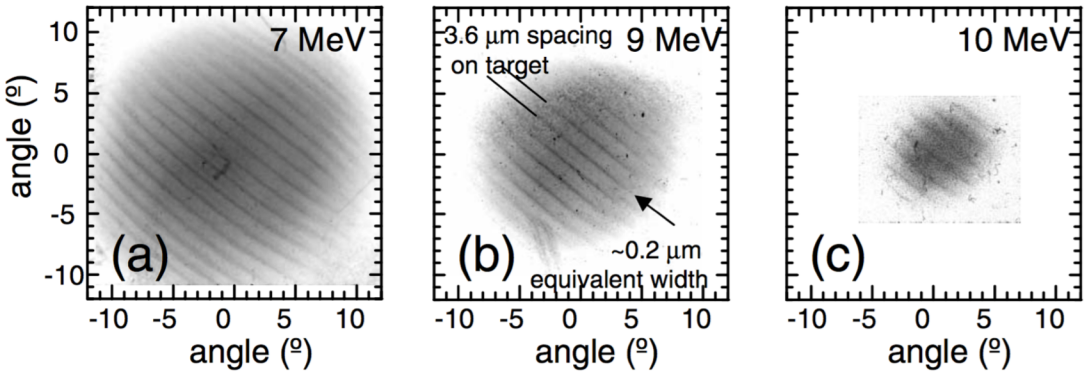

Transverse emittance <0:004 mmmrad

Protons are accelerated from a relatively large surface area: Actual source size ~< 70 µm (energy dependent)

Effective source size < 15 µm

TNSA proton beam properties: Virtual source size

M. Borghesi, et al, PRL, 92, 055003 (2004)

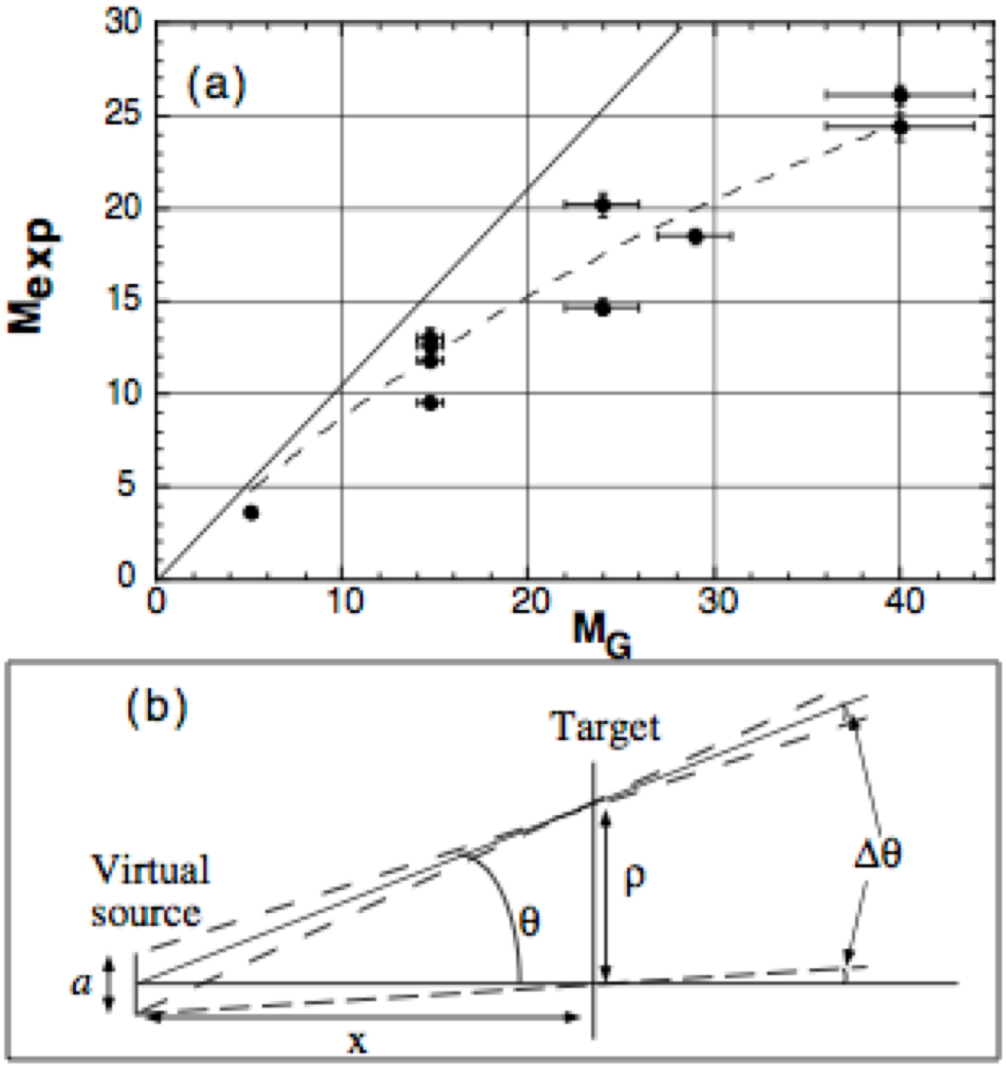

Effective/virtual source size < 10 µm

Spatial resolution for imaging is very good!

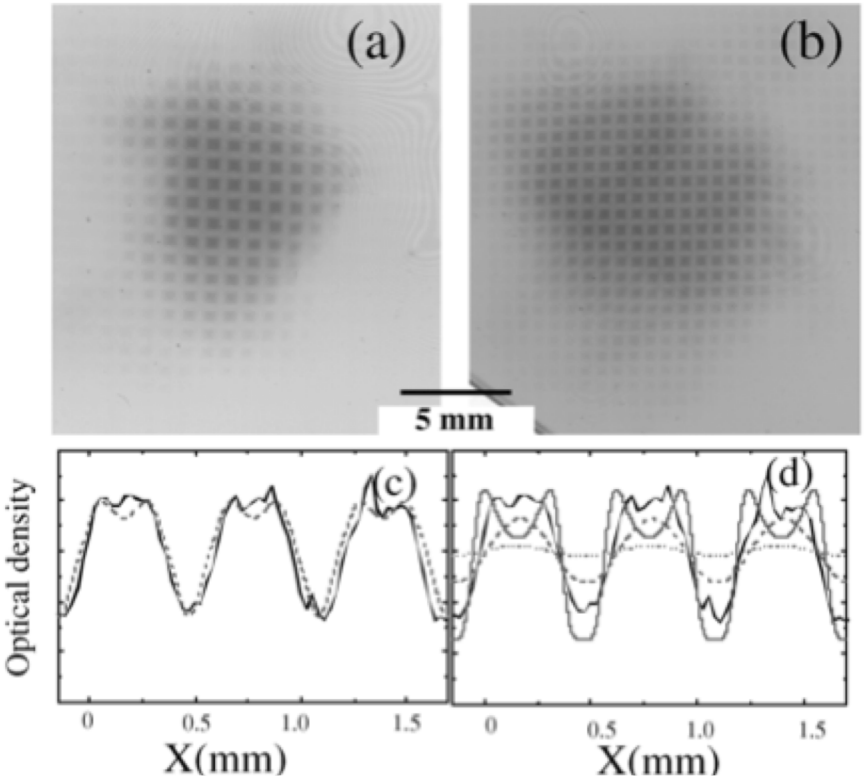

TNSA proton beam properties: Conversion efficiency

J Fuchs, et al., 2, 48, Nature Physics (2006)

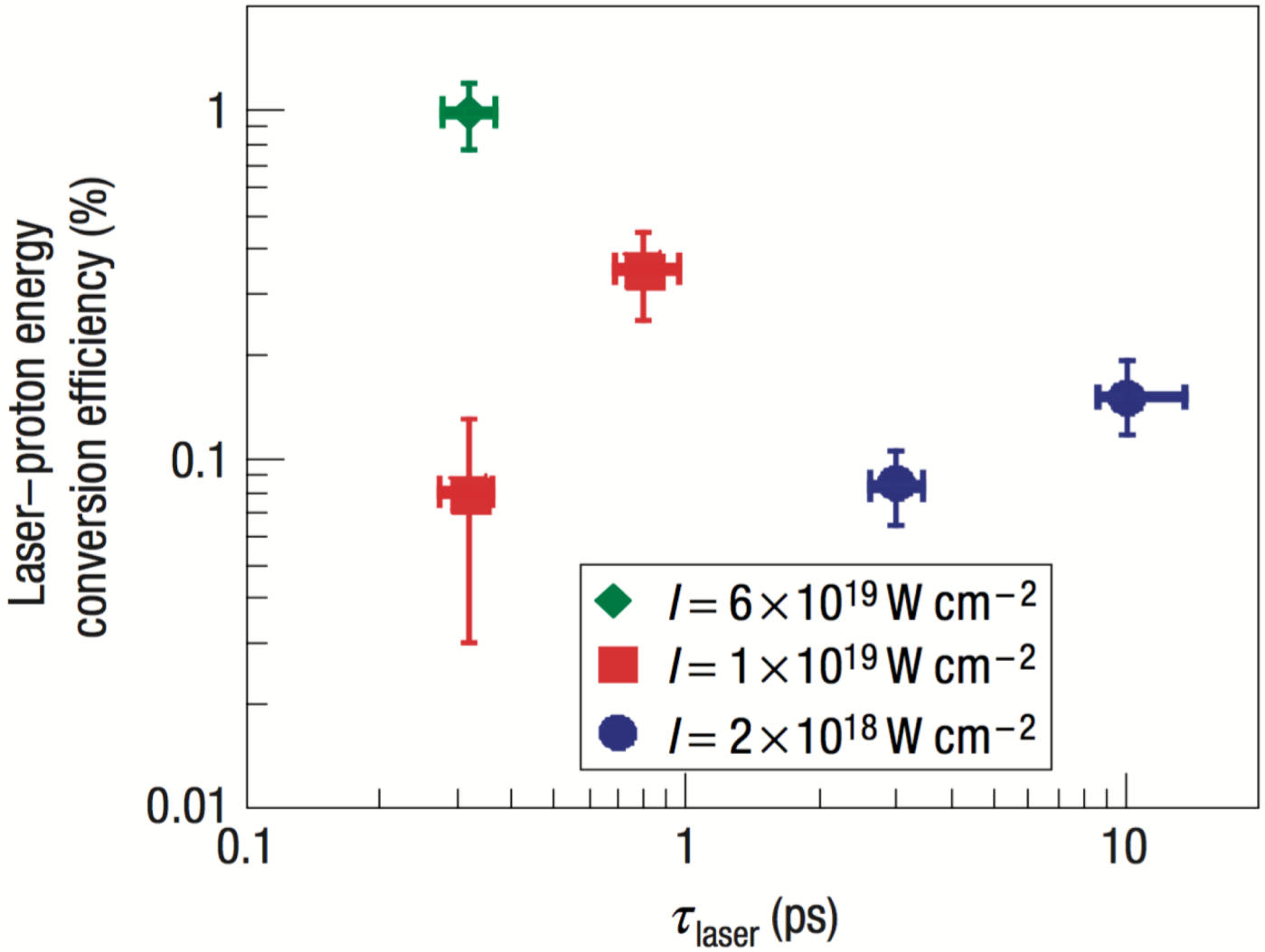

Typical is 1-3%.

Snavely PRL (2000) reported 12%

Laser pulse contrast

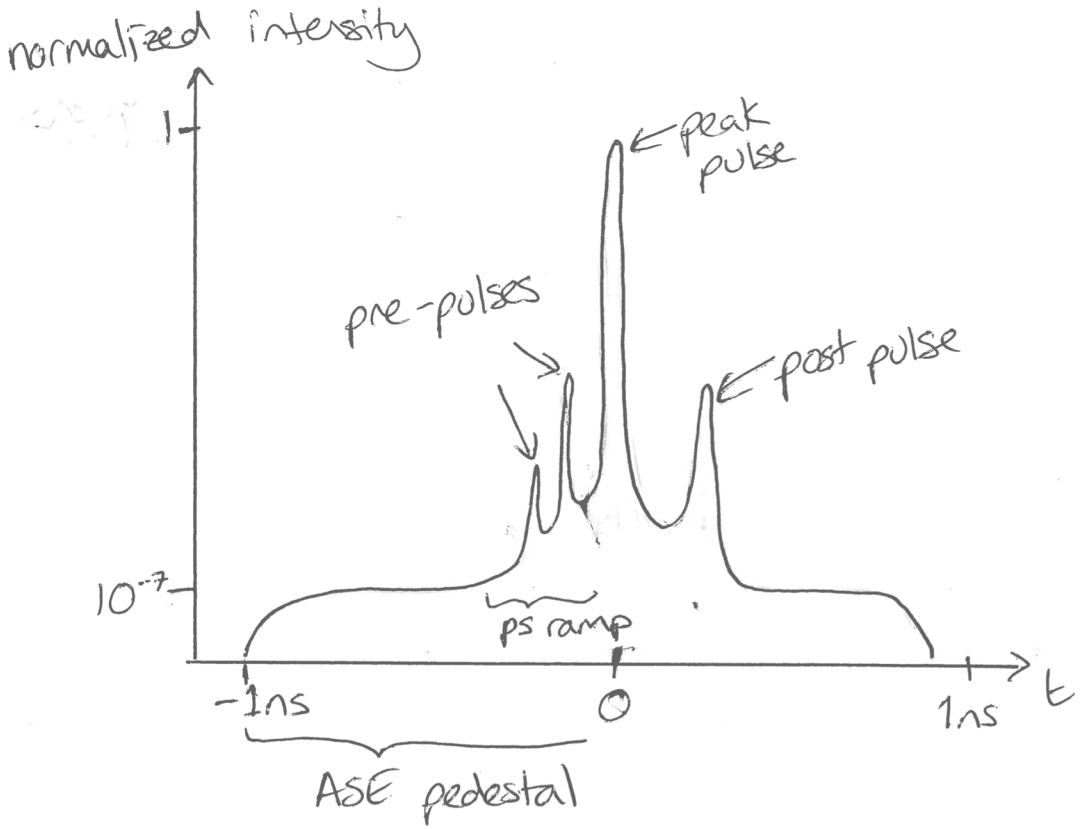

ASE = Amplified Spontaneous Emission

V Chvykov et al. Optics Letters, 31, 1451 (2006)

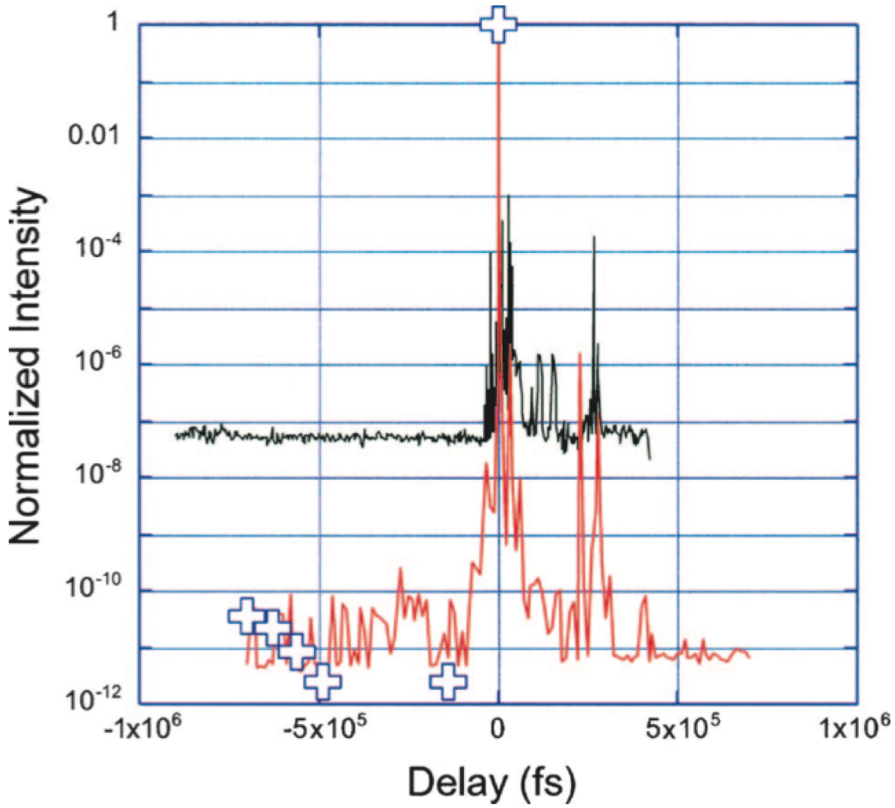

ASE can be intense enough to preform plasma on the front surface of the target:

- Can change the electron absorption
- Shock can breakout of the rear surface and alter rear side density scalelength…

Rear side pre-plasma TNSA inhibition

Preheating of the target can lead to shock breakout on the rear surface. Instead of the sharp vacuum interface a plasma scalelength grows and effectively shorts out the accelerating field when the hot electrons arrive.

MC Kaluza, et al., PRL, 93, 045003 (2004)

Depending on the duration and strength of the ASE prepulse, there is an optimum target thickness for TNSA acceleration

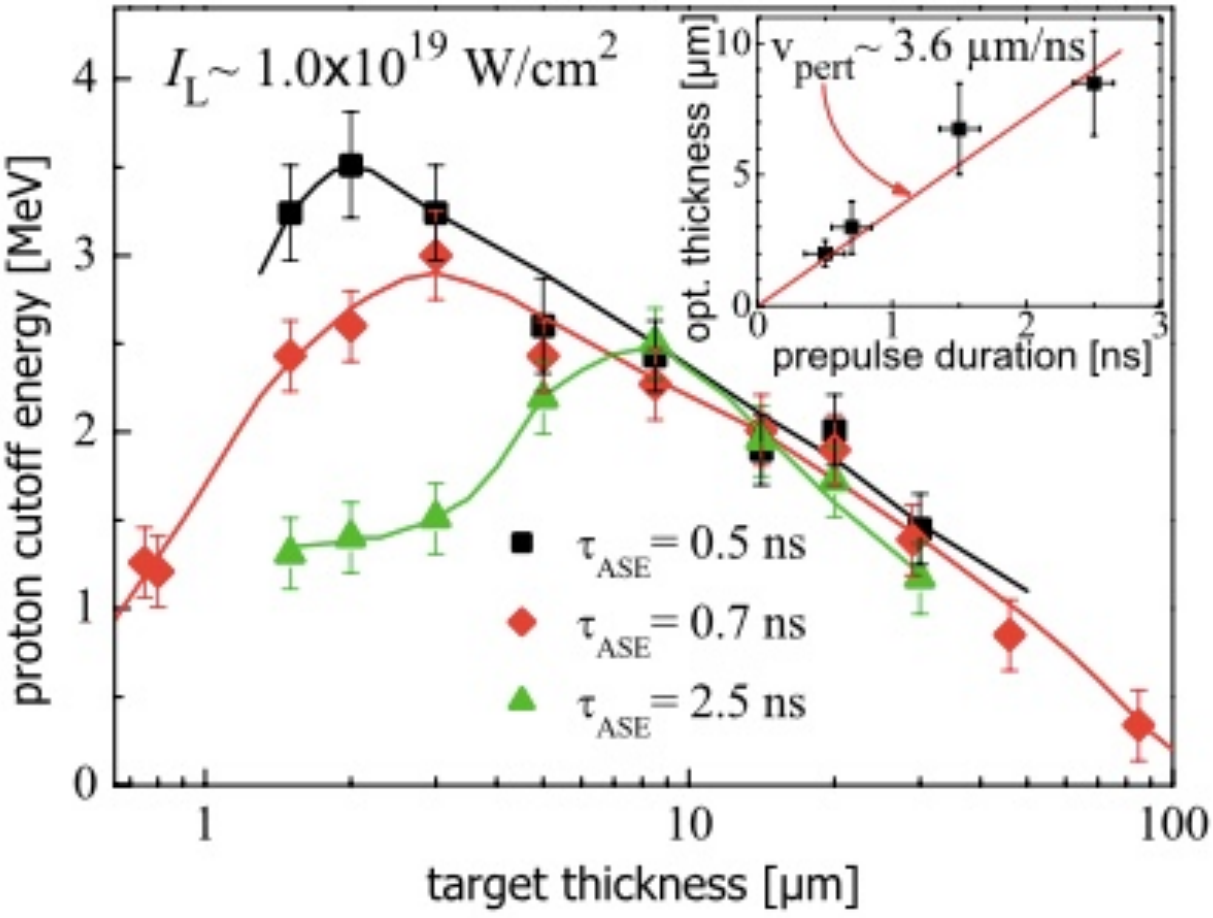

Rear side pre-plasma TNSA inhibition

MC Kaluza, et al., PRL, 93, 045003 (2004)

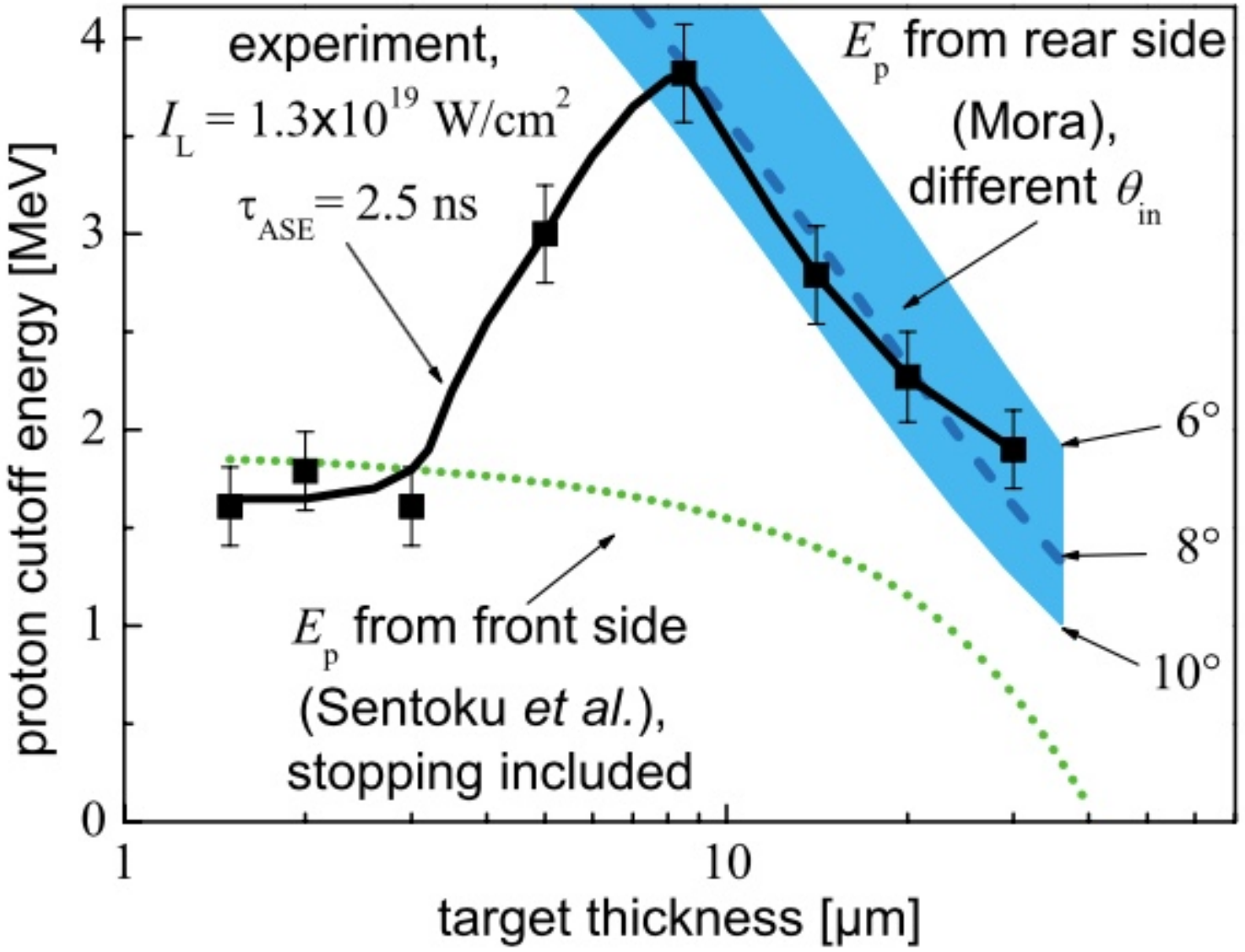

Laser contrast enhancement: Plasma mirrors

P Gibbon, 3, 369, Nature Physics (2007)

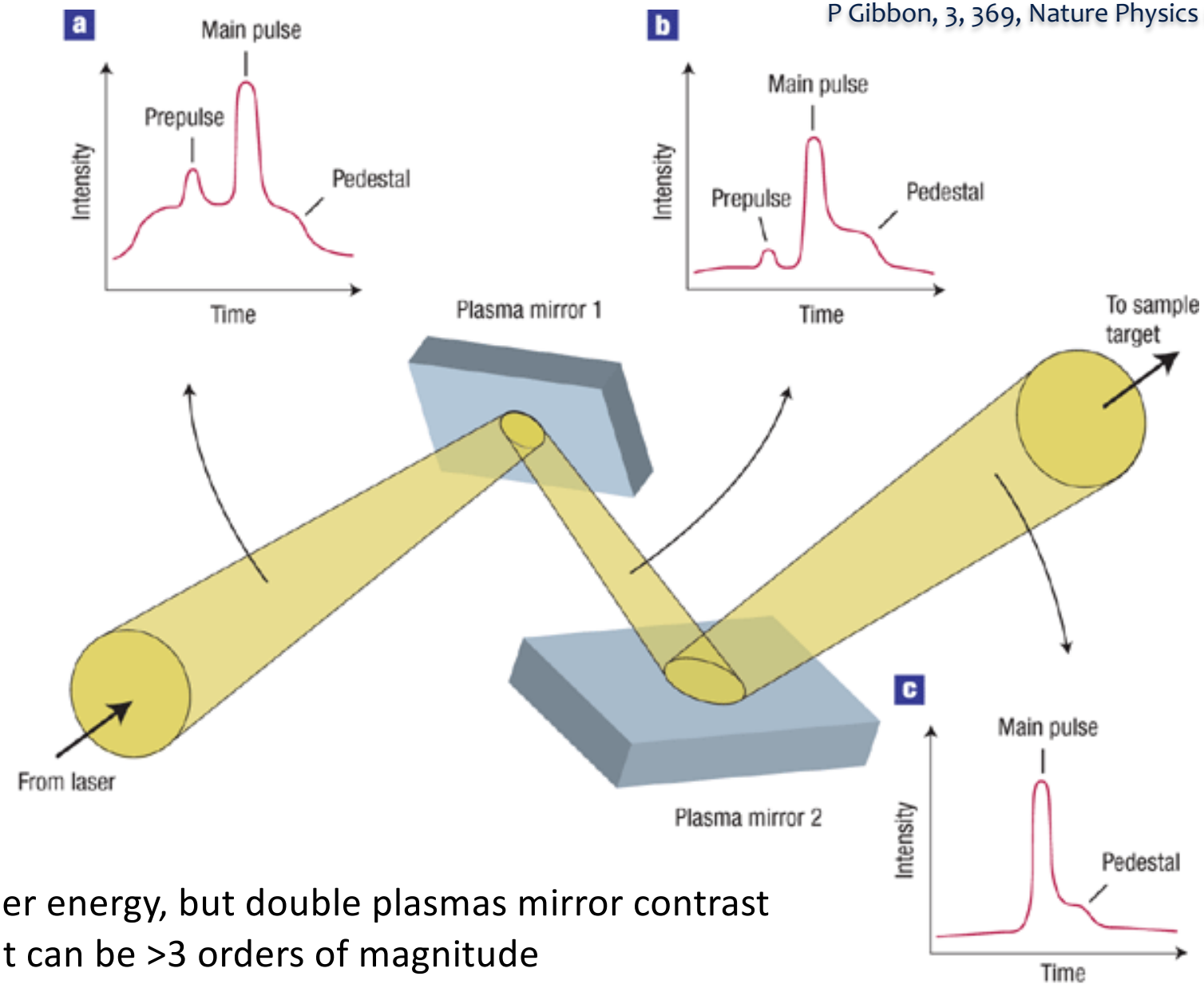

Lose total laser energy, but double plasmas mirror contrast enhancement can be >3 orders of magnitude

Laser-driven ion beam applications: Proton Radiography

M Borghesi et al, Rev Sci Inst, 74, 1688 (2003); Laser and Part Beams, 20, 269 (2002)

Proton beam is accelerated (via TNSA):

Laminar acceleration – good spatial resolution

Short acceleration time – good temporal resolution

Maxwellian-like spectra

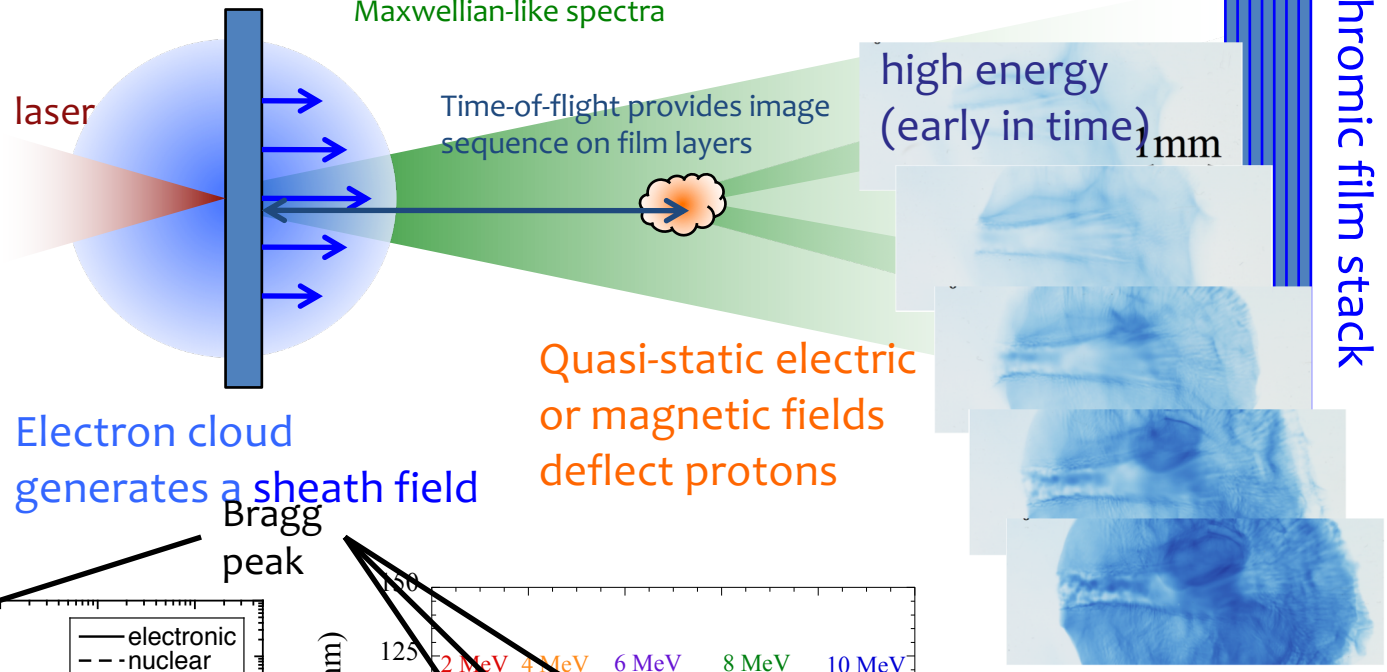

Bragg peak

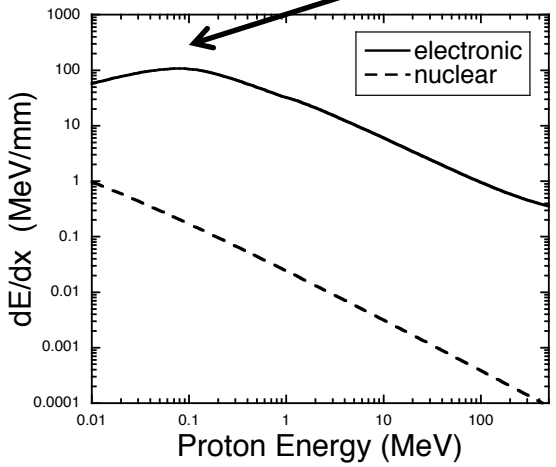

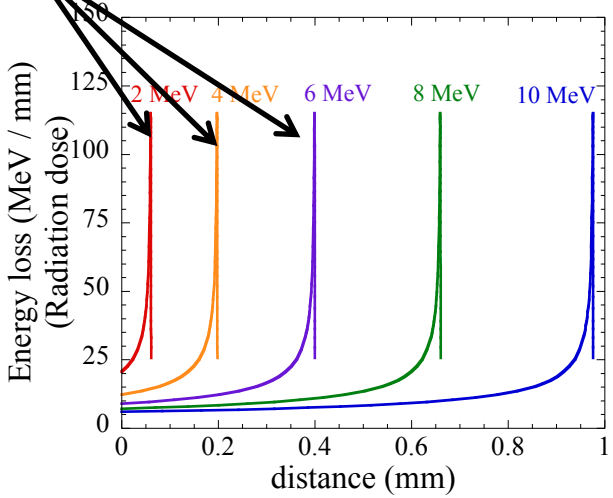

Laser-driven ion beam applications: Proton Radiography examples

Ultrafast field propagation
K Quinn *et al*, PRL, 102, 194801 (2009)

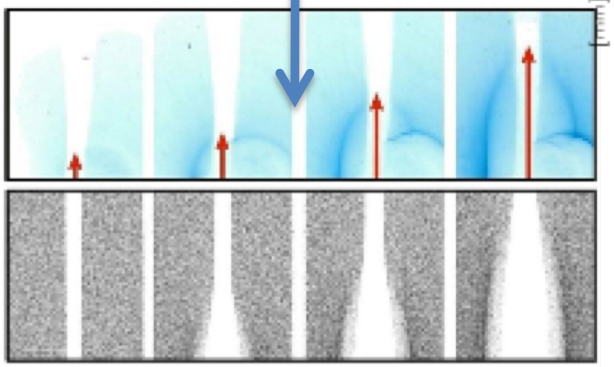

Plasma evolution in laser wake
M Borghesi *et al*, PRL, 94, 195003 (2005)

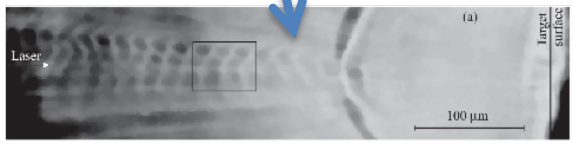

Relativistic electron propagation
B Ramakrishna *et al*, Astrophys Space Sci, 322, 161 (2008)

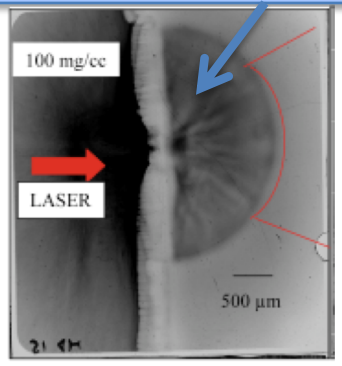

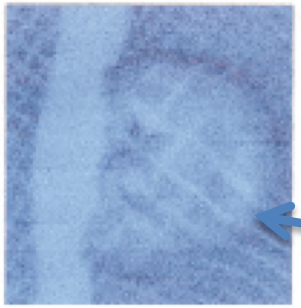

Plasma and field evolution
AJ MacKinnon *et al*, Rev Sci Inst, 75, 3531 (2005)

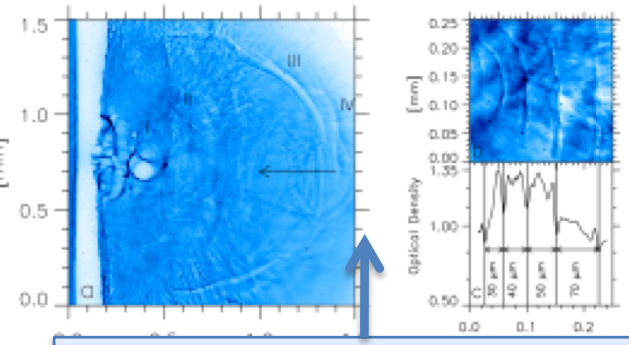

Collisionless shocks
L Romagnani *et al*, PRL, 101, 025004 (2008)

Proton Radiography

Soliton formation
M Borghesi *et al*, PRL, 88, 135002 (2002)

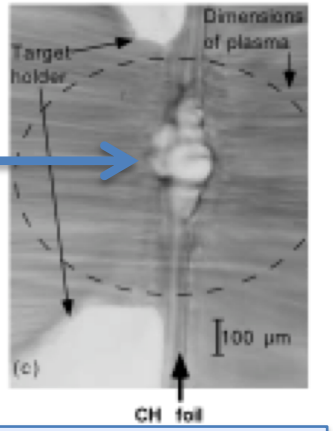

Channel formation imaging in underdense plasma
S Kar *et al*, New Journal of Physics, 9, 402 (2007)

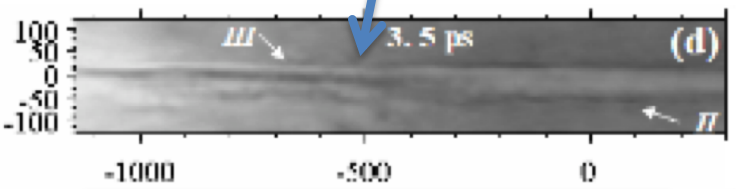

Magnetic reconnection
L Willingale *et al*, PoP, **17**, 043104 (2010)

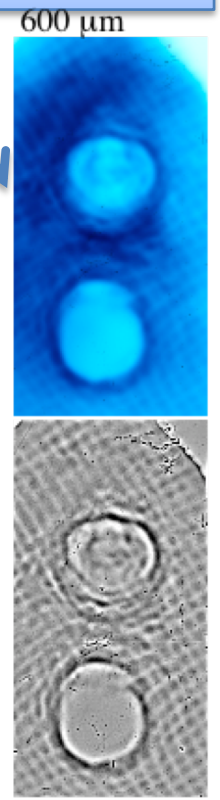

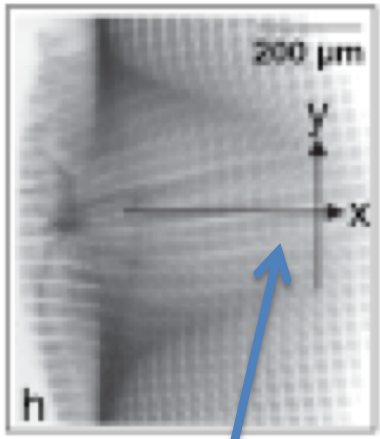

Proton acceleration fronts
L Romagnani *et al*, PRL, 95, 195001 (2008)

Laser-driven ion beam applications: Neutron beam generation

Example reactions

- D + D → ^{3}He + n Q = 3.27 MeV
- D + ^{7}Li → ^{8}Be + n Q = 15.03 MeV
- p + ^{7}Li → ^{7}Be + n Q = -1.64 MeV

Center-of-mass neutron energy can be upshifted due to initial beam energy → directional neutron beam

→ generated on time-scale of several picoseconds

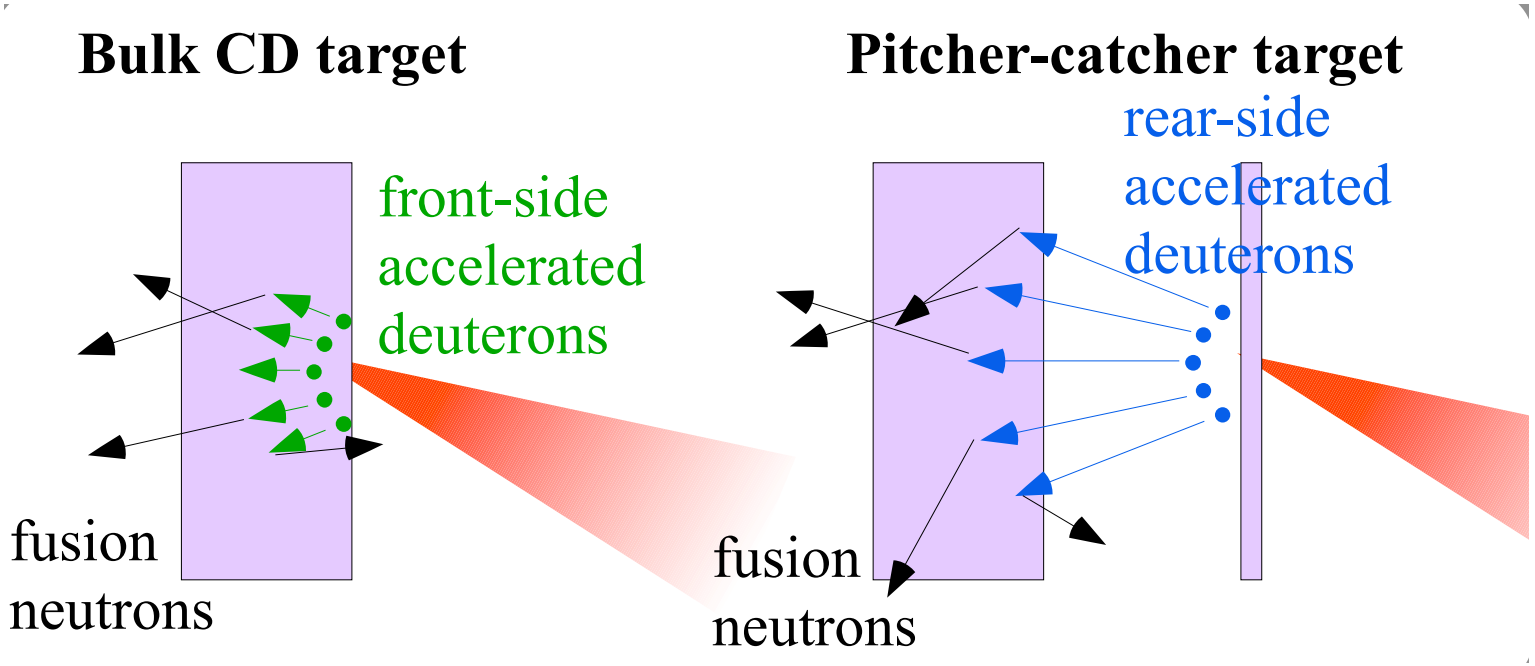

Laser-driven ion beam applications: Beam transport (for experiments like cell irradiation)

Proton acceleration studies with ultrashort PW pulses at DRACO

F.-E. Brack, L. Gaus, A. Jahn, S. Kraft, F. Kroll, J. Metzkes, L. Obst, M. Rehwald, **H.-P. Schlenvoigt**, K. Zeil, T. Ziegler, U. Schramm, T. Cowan, S. Bock, C. Eisenmann, R. Gebhardt, U. Helbig, D. Möller, E. Beyreuther, L. Karsch, M. Schürer, J. Pawelke, T. Herrmannsdörfer, S. Zherlitsyn, S. Goede, M. Gauthier, W. Shoemaker, S. Glenzer, P. Poole, G. Cochran, D. Schumacher

- DRACO: a 150 TW / 1 PW dual beam laser facility
- Status of proton acceleration at DRACO
- Highly efficient proton beam transport with pulsed solenoid coils
- Spectral and spatial beam shaping for in-vivo radiobiology studies

EAAC 2017

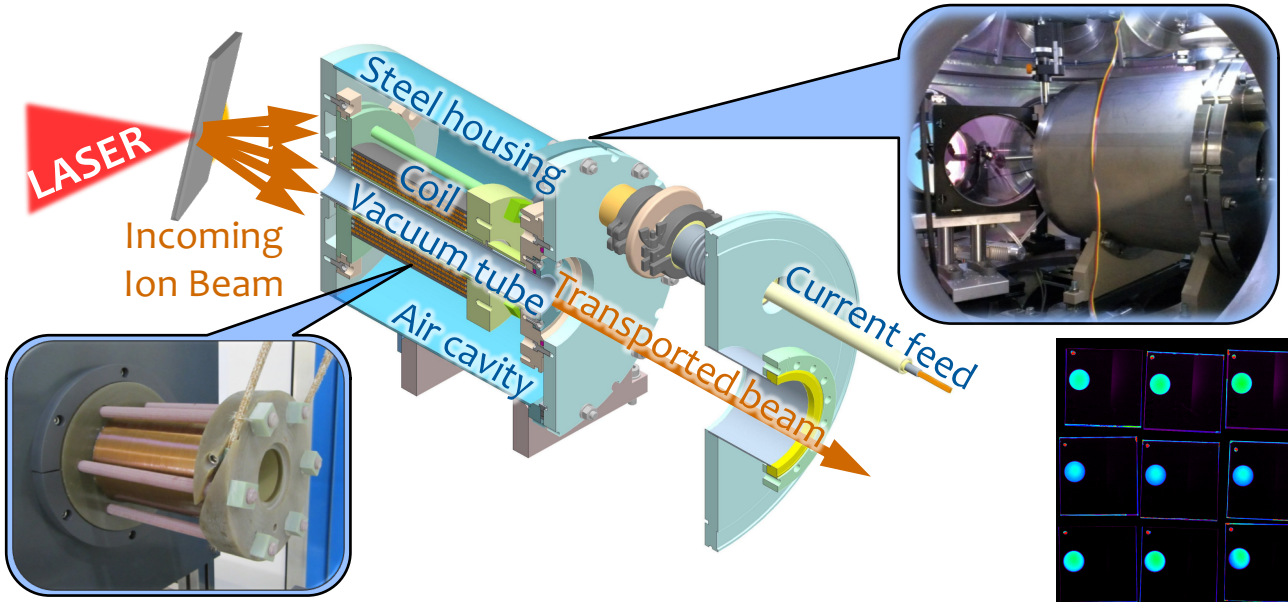

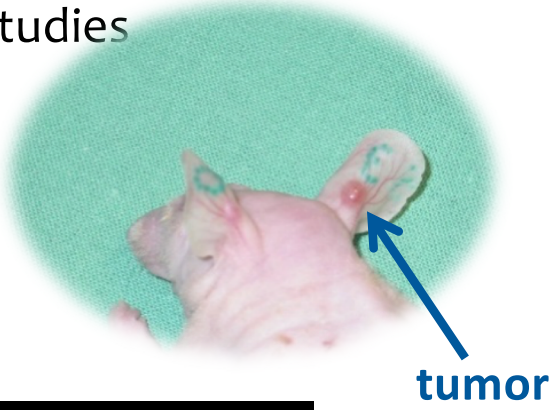

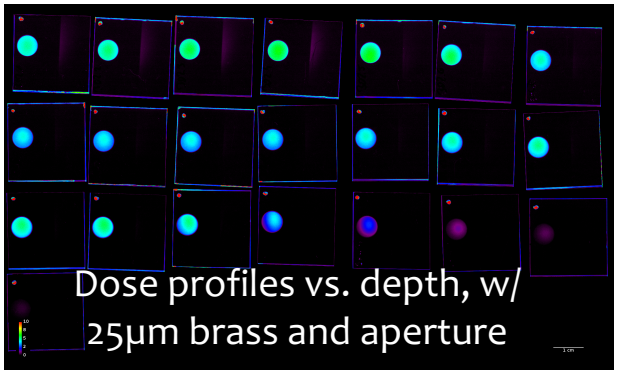

HLD. OncoRay National Center for Radiation Research in Oncology Dresden SLAC The Ohio State University HZDR

Louise Willingale
The CERN Accelerator School, High Gradient Wakefield Accelerators
Sesimbra, Portugal, 18th February 2019

Laser driven ion and proton acceleration

- Acceleration mechanism summary
  - Target Normal Sheath Acceleration (TNSA)
  - Advanced mechanisms: RPA, BOA, Magnetic vortex, Shock
- Common physics themes
- Theoretical models to describe TNSA
- Electron heating and fast electron transport
- Proton and ion diagnostics
- TNSA proton beam properties, scaling and other effects
- Laser-driven proton beam application examples

TNSA

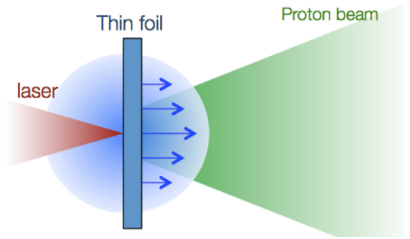

RPA

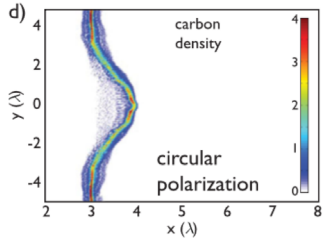

BOA

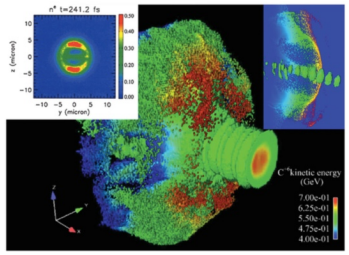

Magnetic vortex

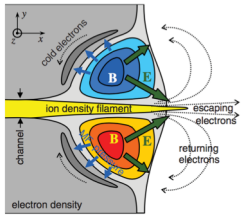

Shock